ELSEVIER

Contents lists available at ScienceDirect

### Desalination

journal homepage: www.elsevier.com/locate/desal





## Polyelectrolyte metallopolymer particles for efficient PFAS capture and release<sup>★</sup>

Till Rittner <sup>a,1</sup>, Kevin Staudt <sup>b,1</sup>, Blandine Boßmann <sup>a</sup>, Ralf Kautenburger <sup>c</sup>, Jean G.A. Ruthes <sup>d,e</sup>, Christopher W.M. Kay <sup>b,f</sup>, Volker Presser <sup>d,e,g</sup>, Horst P. Beck <sup>h</sup>, Markus Gallei <sup>a,g,\*</sup>

- <sup>a</sup> Polymer Chemistry, Saarland University, Campus C4 2, 66123 Saarbrücken, Germany
- <sup>b</sup> Physical Chemistry and Chemistry Education, Saarland University, Campus B2 2, 66123 Saarbrücken, Germany
- <sup>c</sup> Inorganic Solid-State Chemistry, Elemental Analysis Group, Saarland University, Campus C4 1, 66123 Saarbrücken, Germany
- <sup>d</sup> INM-Leibniz Institute for New Materials, Campus D2 2, 66123 Saarbrücken, Germany
- <sup>e</sup> Department of Materials Science and Engineering, Saarland University, Campus D2 2, 66123 Saarbrücken, Germany
- f London Centre for Nanotechnology, University College London, 17-19 Gordon Street, London WC1H OAH, United Kingdom
- g saarene, Saarland Center for Energy Materials and Sustainability, Campus C4 2, 66123 Saarbrücken, Germany
- <sup>h</sup> Inorganic and Analytical Chemistry, Campus Dudweiler Beethovenstrasse Zeile 4, Saarland University, 66125 Saarbrücken, Germany

#### HIGHLIGHTS

- Two efficient approaches for the preparation of porous organic microparticles with cobaltocenium-based functionalities
- $\bullet$  Reversible adsorption of PFOA and PFOS of up to 97 % for PFOA and PFOS at low concentrations of 20  $\mu g \ L^{-1}$
- Elucidating the mechanism for PFOA adsorption and confirmation of a BET mechanism

### ARTICLE INFO

# Keywords: PFAS Metallopolymers Polyelectrolytes Porous materials Separation technologies

### ABSTRACT

In technologies for PFAS removal, one of the biggest challenges is combining high adsorption capacity with excellent regeneration capabilities. In recent years, metallopolymer-based materials have shown promising potential in both aspects. In this work, we present two convenient ways to functionalize organic microparticles with charged, functional moieties (cobaltocenium), either through a one-pot reaction via siloxane-condensation or by straightforward ring-opening reaction of epoxides. After characterization of the novel adsorbent materials by state-of-the-art analytics to verify the successful functionalization, their performance for PFAS adsorption and regeneration was investigated. To gain insight into the adsorption mechanism, experiments were first conducted at low concentrations (20  $\mu g \ L^{-1}$ ) and in equilibrium, showing adsorption for both materials of up to 97 % for PFOA and PFOS. Furthermore, an increase in adsorption within an ionic matrix of commercial drinking water and an adsorbent preference at different pH values was demonstrated. Analysis of the influence of the concentration indicates multilayer adsorption beyond simple ion-paring, best described by a Brunauer-Emmett-Teller mechanism. Moreover, utilizing a straightforward column setup, the total PFOA capacity is analyzed, revealing a 4–5-fold increase upon functionalization, leading to 215 mg g $^{-1}$  and 296 mg g $^{-1}$  PFOA adsorption. Overall, column-based adsorption experiments showed promising results at low (20  $\mu g \ L^{-1}$ ) and medium (2.25 mg  $L^{-1}$ ) PFAS concentrations. Finally, reusability and regeneration studies further revealed an excellent desorption performance upon multiple cycles and PFAS elution of up to 88  $\pm$  4 %.

<sup>\*</sup> This article is part of a special issue entitled: 'Desalination technology' published in Desalination.

<sup>\*</sup> Corresponding author at: Polymer Chemistry, Saarland University, Campus C4 2, 66123 Saarbrücken, Germany. E-mail address: markus.gallei@uni-saarland.de (M. Gallei).

<sup>&</sup>lt;sup>1</sup> Till Rittner and Kevin Staudt are co-first authors contributing equally to this work.

#### 1. Introduction

The presence of poly- and perfluorinated substances (PFAS) in water sources is a topic of growing scientific interest. Initially utilized for their omniphobic properties, these compounds are employed in a plethora of industrial and consumer products, including packaging, electronics, lubricants, firefighting foams, cosmetics, and water-repellent sportswear [1]. These materials chemically contain highly stable C—F bonds, which is the molecular prerequisite for their desired interesting properties. This high C—F-bond stability represents one of the greatest challenges, as the absence of perfluorinated substances produced in nature results in the inability of biological organisms to degrade them [2].

Consequently, PFAS accumulates in the environment from waste or industrial runoff and can now be found in every location on Earth [3]. One significant distribution pathway is via freshwater and irrigation technologies [4], which results in contamination of drinking water and human exposure to PFAS. As evidenced by recent literature, PFAS can accumulate in the human bloodstream and cause significant health and fertility issues [5,6]. However, due to the ubiquitous aqueous availability of these compounds in concentrations ranging from single to several hundred nanograms per liter, removal and destruction are challenging [7].

Generally, degradation of the pollutants requires energy or chemical inputs. Preconcentration has to be performed first [7,8]. As is customary in water purification, the initial stage involves the utilization of activated carbon or silicate-based materials [9,10]. Despite the high surface area of these materials, the lack of regeneration opportunities results in a significant waste of adsorption materials, which are not capable of releasing PFAS. Other carbon-based materials, including carbon nanotubes and molecularly imprinted polymers, have been investigated for PFAS sorption and regeneration capabilities [11-13]. These systems, which were focused on weak alternating effects, were superseded by more targeted methodologies. Studies documented in literature predominantly focused on the two principal components of the vast array of perfluorooctanoic acid (PFOA) namely fluorooctanesulfonic acid (PFOS) [14-16], as these compounds possess the typical chemical structure of the majority of perfluorinated degradation products.

In recent years, in order to develop feasible adsorption materials, there has been an emphasis on the interaction of adsorption with perfluorocarboxylic acid. A significant proportion of this research is dedicated to the selective fluorine-fluorine interaction, which is typically relatively weak but possesses a distinctive nature compared to other impurities [17]. As a result, numerous membrane and other materials have been developed [18]. In addition to this relatively weak F-F interaction, a somewhat stronger aromatic interaction is also known [19]; however, this feature receives less attention due to its nonselectivity. In direct contrast, the ionic interaction is of particular interest [20,21]. Given that a significant proportion of the compounds to be removed possess ionic characteristics, the strong Coulombic interaction enables the effective capture of PFAS [22], and ion exchange resins or gels are particularly well-suited for this purpose [23,24]. However, the disadvantages are the high cost and poor regeneration of these materials [25,26]. Another emerging class of inorganic adsorbents are metal-organic frameworks (MOFs) and MXenes, which excel due to nanostructured surfaces or layered structures [27,28].

Recently, new materials based on metallocenes were introduced, which show some significant advantages [29]. The molecular motifs, which combine an organic, aromatic backbone with a metallic, inorganic core, offer a distinctive electronic configuration that facilitates the chemical or electrical switching of the metallo-component, resulting in a change of the charged state [30]. In the literature, a huge variety of applications is known for polymers and surfaces featuring metallocenes [31–39].

In a PFAS adsorption study, the metallocene polymer-based materials demonstrated a high affinity and effective desorption following

electrical switching [29]. Materials based on cobaltocenium were particularly amenable to this purpose. Cobaltocenium, naturally existing as an aromatic cation, exhibits a very strong interaction with PFAS [29]. However, to date, immobilization, such as covalent bonding of the metallocene material onto a functional substrate, was difficult to achieve, especially for the unreactive cobaltocenium.

One step towards addressing this issue is our recent approach to attach cobaltocenium via catalyst-free hydroamination of ethynyl cobaltocenium onto an amine-containing block copolymer. By this, highly defined block copolymers with tailorable cobaltocenium content were prepared, showing self-assembly and electric addressability [40]. Based on these polymers, our group was recently able to develop a membrane with a high PFAS retention at low pressures, proving the viability of cobaltocenium-based materials for adsorption [41]. However, for this system, reusability was limited due to swelling upon interactions with different solvents, which is required for regeneration of the membrane, limiting real-life applicability. Furthermore, the adsorption process itself and the underlying interactions of the adsorption mechanism were yet to be determined.

The present study aims to gain further insight into the interaction and adsorption mechanism between cobaltocenium and PFAS. Furthermore, to emphasize reusability and regeneration, we focus on a less solvent-dependent particle-based system by functionalizing commercially available polystyrene-divinylbenzene (PSDVB) particles with cobaltocenium moieties.

The objective is to investigate the amount of cobaltocenium introduced, the type of functionalization employed, and its effect on the PFAS adsorption process. Two functionalization strategies are proposed for investigation, utilizing either siloxane-condensation reactions or epoxide ring-opening strategies at the surface of the particles. Moreover, the interaction between the synthesized materials and the two prominent representatives, PFOA and PFOS, was investigated to gain insights into the performance and capability of PFAS removal and regeneration over a range of experimental conditions comprising the water matrix, pH value, and different perfluorinated compound concentrations. By analyzing the adsorption at equilibrium, the adsorption mechanism will be determined for the first time. Finally, a flow-based setup was developed to increase the capacity and regeneration of the adsorbed PFAS from the substrate. The insights presented here pave the way for a new class of metallocene-based PFAS adsorbents with excellent adsorption and regeneration capabilities.

### 2. Materials and methods

### 2.1. Materials

All solvents and reagents were purchased from Alfa Aesar, Sigma-Aldrich, Fisher Scientific, ABCR and used as received unless otherwise stated. Ethynyl cobaltocenium was synthesized according to a literature procedure [42]. PSDVB particles were generously provided by Metrohm. Water, acetonitrile, methanol (HPLC grade), and ammonium hydroxide were obtained from VWR. Perfluorooctanoic acid (PFOA), perfluorooctanesulfonic acid (PFOS), acetic acid, and sodium hydroxide were obtained from Sigma Aldrich.  $^{13}\mathrm{C_8}\text{-Perflourooctanoic}$  acid ( $^{13}\mathrm{C-PFOA}$ ) (50  $\mu\mathrm{g}$  mL $^{-1}$  in methanol) and  $^{13}\mathrm{C_8}\text{-perflourooctanesulfonic}$  acid ( $^{13}\mathrm{C-PFOS}$ ) (50  $\mu\mathrm{g}$  mL $^{-1}$  in methanol) were obtained from Wellington Laboratories and distributed by Campro Scientific.

### 2.2. Instrumentation

### 2.2.1. Particle analysis

Infrared (IR) spectra were recorded on a BRUKER ALPHA II FT-IR spectroscopy setup in attenuated total reflection mode (ATR) with spectrum output in transmittance. All spectra were processed with OPUS 8.5 (SP1) software (baseline correction) and Origin2020b (normalized).

Thermogravimetric analysis (TGA) was performed using a Netzsch

TG 209 F1 Libra with a heating rate of 10 K min $^{-1}$ , nitrogen as protective gas, and synthetic air as a purge gas with a flow rate of 20 mL min $^{-1}$ . For evaluation, Netzsch Proteus Thermal Analysis software 8.0.1 was used.

Scanning electron microscopy (SEM) was performed on a Zeiss Sigma VP device (GeminiSEM 500) using the SmartSEM Version 6.07 software. The samples were mounted on an aluminum stud with adhesive carbon tape and sputter-coated with approximately 6 nm platinum using an Automatic Turbo Coater PLASMATOOL 125 SIN 2020\_131 from Ingenieurbüro Peter Liebscher.

For ICP-MS measurements, inductively coupled plasma triple quadrupole mass spectrometry (Agilent 8900 ICP-QQQ, Santa Clara, USA) was used. For sample preparation, 10 mg of particles were reacted with aqua regia for 24 h at 60 °C. The solutions were quantitatively transferred in 50 mL polypropylene (PP) volumetric flasks (BRAND GmbH & Co. KG). Ultrapure water (0.055 μS cm<sup>-1</sup>) from a PURELAB® Chorus 1 ultrapure water filtration unit (Elga LabWater) was used to prepare all solutions. From each of these solutions, 50 µL were taken and prepared as 10 mL measurement solutions (dilution factor: 200). A solution containing 10 mg  $L^{-1}$  each of Sc (1 g  $L^{-1}$  in 5 % HNO<sub>3</sub>, Alfa®), Y (1 g  $L^{-1}$ in 2-3 % HNO<sub>3</sub>, Merck Certipur®) and Ho (1 g L-1 in 2-3 % HNO<sub>3</sub>, Merck Certipur®) in ultrapure water was prepared as an internal standard solution for all ICP-MS measurements. HNO<sub>3</sub> (69 %, ROTIPURAN® Supra, Carl Roth) was used to acidify the measurement solutions. Argon 5.0 (Ar  $\geq$  99.999 mol%, ALPHAGAZ<sup>TM</sup> 1 Argon, Air Liquide) was used as plasma gas for ICP-MS measurements. An external calibration was prepared using Co (1 g L<sup>-1</sup> in 0.005 M HNO<sub>3</sub>, Fluka) ICP-MS standard solutions for quantification.

Nitrogen sorption analysis was carried out with utmost thoroughness using an Autosorb IQ system (Anton Paar) at  $-196\,^{\circ}\text{C}$ . Before each measurement, the samples were outgassed for 5 h at 100  $^{\circ}\text{C}$  under a vacuum, ensuring the removal of any residual gases. The Brunauer-Emmett-Teller (BET) theory was applied to determine the cumulative specific surface area.

### 2.2.2. PFAS analysis

Ion chromatography (IC) was performed on a Metrohm Compact IC Flex equipped with an 800 Dosino and 858 Professional Sample Processor. For PFOA analysis, the Metrohm Application 8.000.9053EN for "Trace-level detection of perfluorinated compounds in water by suppressed ion chromatography with inline suppression" was used with slight variations. In more detail, separation was achieved by isocratic elution on a reversed-phase column thermostated at 35 °C using an aqueous mobile phase containing boric acid and acetonitrile. For the column, a NUCLEODUR 100-5 C18 ec, 5  $\mu m$ , 125  $\times$  4.6 mm from Macherey-Nagel was used. For the eluent, 20 mmol L $^{-1}$  boronic acid and 4 mmol L $^{-1}$  NaOH (pH-adjusted to 8) in 35 % acetonitrile were used. The flow rate was set to 1 mL min $^{-1}$  with an injection volume of 200  $\mu L$ . Boronic acid and sodium hydroxide EMSURE from Merck and perfluorooctanoic acid (PFOA) (96 %) from Thermo Scientific were used.

For LC-MS measurements, samples were first prepared by solid phase extraction (SPE) using BEKOlut PFAS WAX cartridges (6 mL, 150 mg) (CS Chromatography Service GmbH). SPE chambers were obtained from Macherey-Nagel and Varian. The Engineering Workshop of Saarland University constructed the custom-made evaporation chamber. Chromatographic separation was achieved by a Shimadzu LC20-AD-XR-system containing a degasser (DGU-20A3), 3 HPLC pumps (2 precolumn (LC20AD-XR), 1 post-column (LC40D-XR)), autosampler (SIL-20AC-XR) and a column oven (CTO-20AC). In all experiments, a Multospher 120 RP18-AQ-3µ was used for chemical separation (CS Chromatographie Service GmbH). The HPLC was coupled with a solariX 7T FT-ICR-mass spectrometer (Bruker Daltonics GmbH & Co. KG) with ftms control 2.3.0 and Compass HyStar 5.1.8.1 software for data acquisition and Compass Data Analysis 6.0 for Data processing.

#### 2.3. PSDVB particle modifications

### 2.3.1. Siloxane-based particles (PSDVB@APTES-Co)

The synthesis was accomplished according to the literature [42]. In brief, in a three-neck flask with a KPG stirrer, reflux condenser, and rubber septum, ethynyl cobaltocenium hexafluorophosphate (6.0 g, 16.5 mmol, 1.0 eq) was dissolved in 750 mL dry acetonitrile (ACN). 3-aminopropyl ethyl siloxane (APTES) (3.7 g, 16.5 mmol, 1.0 eq) was added, and the reaction was stirred at 50 °C for 24 h. After 30 min, a deep red color was noticeable. Next, the hydroxy-functionalized PSDVB (6.0 g) particles were added, and the reaction was stirred for 72 h at 80 °C. Particle samples (2 mL of solution) were taken periodically for kinetic analysis. The functionalized particles were filtered using a 1.6  $\mu$ m glass microfilter and washed via several intervals of centrifugation and redispersion in excess of ACN, acetone, and tetrahydrofuran (THF). After drying in a vacuum at 40 °C overnight, 6.8 g of final particles (PSDVB@APTES-Co) were obtained.

### 2.3.2. Epoxy-based particles (PSDV@epoxy-Co)

In a three-neck flask with a KPG stirrer, PSDVB particles (12.0 g) and 700 mL dichloromethane (DCM) were added and cooled to 0 °C by using an ice bath. Meta-chloro perbenzoic acid (mCPBA) (12.4 g, 50 mmol, 70 mass%) was added carefully. The reaction was slowly adjusted to room temperature and stirred for 4 d. The particles were removed from the reaction solution via centrifugation, followed by purification via redispersion and centrifugation utilizing excess DCM, THF, and acetone. Finally, epoxidized particles were obtained after drying in a vacuum at 40 °C overnight. In the next step, the epoxidized particles (5.0 g) were added to a three-neck flask with a KPG stirrer and reflux condenser. Ethanolamine (200 mL) and toluene (400 mL) were added. The reaction was stirred at reflux for 48 h, and the resulting particles were removed by centrifugation. The crude particles were purified, as noted before, by utilizing an excess (~500 mL) of toluene, THF, and acetone. 5.07 g of aminated particles were obtained after drying in a vacuum at 40 °C overnight. For the final step, aminated particles (5.0 g) were added to a 500 mL three-neck flask with a KPG stirrer and reflux condenser. Dry ACN (250 mL) and ethynyl cobaltocenium hexafluorophosphate (2.5 g, 6.98 mmol) were added, and the reaction dispersion was stirred at 80  $^{\circ}$ C for 72 h. The particles were purified by filtration over a 2 μm glass filter and purified by washing with ACN and acetone. After drying in a vacuum at 40 °C overnight, 5.8 g of the final PSDVB@epoxy-Co was obtained.

### 2.4. PFAS adsorption and regeneration studies

### 2.4.1. PFAS detection via LC-MS

2.4.1.1. Adsorption tests. For adsorption measurement at equilibrium, 50 mL of water and ACN (95/5 by volume) per sample were filled in falcons (Sarstedt AG & Co. KG). 1 µg of either PFOS or PFOA were added to the sample, followed by 5 mg of adsorbent material. The resulting suspensions were treated with a thermo shaker (VORTEMP 1550, Nabnet) for 24 h at room temperature, followed by centrifugation (Rotina 420, Hettich Zentrifugen) for 1.5 h at 4500 rpm. The clear supernatant was removed, leaving a 5 mL residue in the suspension. Furthermore, a reference sample was prepared and treated the same way without the addition of the adsorbent, allowing the determination of the sorption efficiency in comparison to the cobaltocenium-modified particle materials. The clear solutions were filled in new vials, adding 200 ng <sup>13</sup>C-PFOS or  $^{13}\mbox{C-PFOA}.$  For subsequent SPE, the WAX cartridges were activated by eluting 2 mL ammoniacal MeOH (0.1 vol%), followed by 2 mL MeOH and 2 mL water. The samples were loaded onto the cartridge with a flow rate of a maximum of 5 mL min<sup>-1</sup> and washed with an additional  $4\ mL$  water. For elution,  $4\ mL$  MeOH and  $4\ mL$  ammoniacal MeOH were used. The fractions were collected in pre-weighted 20 mL vials and

evaporated under nitrogen flow at 40  $^{\circ}$ C to a volume between 250 and 500  $\mu$ L. The mass of the vials determined the residual volume. The extract was transferred into an HPLC vial and adjusted to 500  $\mu$ L with methanol, followed by 490  $\mu$ L water and 10  $\mu$ L of an L-arginine stock solution (10  $\mu$ g mL<sup>-1</sup> in H<sub>2</sub>O). Furthermore, a standard solution was prepared to determine the recovery rate.

2.4.1.2. Investigation of matrix influences. Matrix effects due to the presence of other ions were investigated by analyzing the adsorbent materials with the workflow described in section 1.0 in Milli-Q water/ACN (95/5 by volume) and Evian water (from a commercial 0.5 L polyethylene terephthalate bottle)/ACN (95/5 by volume) as a typical representative of drinking water.

2.4.1.3. Investigation of pH value and concentration effects. To explore the influence of pH on the adsorption efficiency, Milli-Q water/ACN (95/5 by volume) solutions at pH 2, 4, 6, 8, 10, 12, and 14 were prepared using sodium hydroxide and acetic acid for adjustment of the respective pH value. The provided concentrations of PFOS and PFOA and its internal standard were used for the concentration series (Table 1):

2.4.1.4. Flow experiments at low PFOS and PFOA concentrations. In this experiment, a column set-up (see Section 2.4.2.1) with 100 mg of adsorbent material was treated with 80 mL of a 20  $\mu$ g L<sup>-1</sup> PFOS or PFOA solution, and an additional 20 mL was set aside as a reference sample (fraction 1). The eluate was collected in 10 mL portions, giving 8 samples (fractions 2-9). To analyze the regeneration of the adsorbent material, the loaded column was then eluted with 5 mL MeOH and 5 mL ammoniacal MeOH; fractions were collected and combined for subsequent analysis (fraction 10). To determine the respective PFOS or PFOA concentrations, an additional reference containing 2 µg of the analyte in 10 mL MeOH was prepared, matching the maximal possible PFOS or PFOA concentration per fraction (fractions 11, 12). For all fractions, 100 ng internal <sup>13</sup>C standard was added after the column treatment. Fractions 1-10 were prepared by SPE (see Section 2.4.1.1) and evaporated with nitrogen at 40 °C. Fractions 11 and 12 were directly evaporated with nitrogen.

### 2.4.2. PFOA determination using ion chromatography (IC)

2.4.2.1. PFOA total capacity analysis. For total capacity analysis,  $100\,$  mg of subject particles were encased into an experimental column made of a HENKE-JECT syringe (3 mL, Luer, sterile) as the column casing and LABSOLUTE glas micro filters (1.6  $\mu m)$  as the membrane material. A graphical demonstration of the setup used and the experimental column can be found in Supporting Information Fig. S1. For the IC measurement, a feed of 500 mg L $^{-1}$  PFOA in a mixture of 970 mL ultrapure water (18  $M\Omega$  cm) and 30 mL methanol (HPLC grade) was used. To verify the feed concentration without the experimental column attached, the first sample was taken after 5 min of flow equilibration (2 mL min $^{-1}$ ). Then, the column was connected, and samples were taken in intervals of 5 min into pre-weighted glass tubes. For each analysis, 15 samples were taken.

**Table 1**PFOA and PFOS concentrations and their corresponding internal standards used for the concentration series.

C (PFOS; PFOA) (mg $L^{-1}$ )	C ( $^{13}$ C-PFOS; $^{13}$ C-PFOA) (mg L $^{-1}$ )
0.002	0.04
0.02	0.04
0.2	0.04
1	2
2	0.4
5	2
10	2
20	2

The column was then removed, and an additional feed sample was taken to verify the analyte concentration. The exact volume of the samples was determined by weight before being diluted for IC analysis. Here, 30  $\mu$ L of sample solution was diluted in 10 mL of 970/30 H<sub>2</sub>O/MeOH and measured by injection of 200  $\mu$ L thereof. The resulting peak integrals were quantified against a linear standard curve. For calculation of the total PFOA capacity  $S_{PFOA}$ , the measured concentration of each sample  $c_{PFOA,sample}$  was divided by the feed concentration directly before the measurement  $c_{PFOA,feed,t=0}$  to get a percentage of adsorption in a set volume. The percentage was now multiplied by the volume  $v_{sample}$  and respective initial feed concentration  $c_{PFOA,feed}$  (500 mg L<sup>-1</sup>) to acquire the amount of PFOA adsorbed for each sample. The sum of all adsorbed PFOA was then divided by the initial particle amount (100 mg), for comparison of mg per mg  $S_{PFOA,mg}$ .

$$S_{PFOA} = \sum \nu_{sample} \bullet c_{PFOA,feed} \bullet \frac{c_{PFOA,sample}}{c_{PFOA,feed}} \bullet (E1)$$

$$S_{PFOA,mg} = \frac{S_{PFOA}}{m_{outricles}} \tag{E2}$$

2.4.2.2. PFOA column reusability tests. For the reusability tests, columns were prepared as described in Section 2.4.2.1, and a PFOA concentration of  $2.25 \text{ mg L}^{-1}$  was used. After the initial setup equilibration time, a sample of the feed was first taken for every run. The column was attached, and the following four column samples were each collected after 2.5 min with a flow rate of 2 mL min<sup>-1</sup>. After collecting the fourth sample, the column was detached and rinsed with 5 mL of air and 1 mL of pure water. The column was now connected to a syringe pump filled with either ammoniacal methanol (0.1 vol% of aqueous 35 % NH<sub>3</sub>) or ionic methanol (1 mass% NaCl) and eluted with a rate of 1 mL min<sup>-1</sup>. All samples were collected into preweighted IC sampling tubes, and the total volume was calculated by weight. After elution, the column was again rinsed with 5 mL of air, 1 mL of water, and 5 mL of air. During the elution process, the feed was constantly running into a waste container, so no build-up occurred. The next feed sample was taken, and the sampling process was repeated. The collected samples were homogenized and measured directly by IC with an injection volume of  $10 \, \mu L$ . For analysis and presentation, the measured concentrations are converted to corresponding percentages of initial feed, as determined for each run.

### 3. Results and discussion

Metallopolymer-based particles were synthesized to assess the complex dynamics of PFAS adsorption onto the newly developed adsorbent materials. As model substances for the vast class of PFAS. PFOS and PFOA were selected, as they are the main pollutants and wellknown to literature. The feasibility of PFOS or PFOA adsorption was then investigated under equilibrium and flow conditions. The structure of this study is presented in Fig. 1. For the synthesis, two different particle batches consisting of cobaltocenium moieties were prepared by either (i) a siloxane-based one-pot-synthesis, forming a multilayer siloxane network at the surface of the organic microparticles or by (ii) ring-opening reaction of epoxidized microparticles with aminecontaining cobaltocenium derivatives. Both synthesis strategies were compared regarding their PFOS and PFOA adsorption, including the influences of the pH value, varying analyte concentrations, and the presence of matrix-ions in the surrounding environment. Finally, the total capacity, the elution of PFOA, and reusability were investigated.

### 3.1. Metallopolymer particle design

Crosslinked polystyrene-divinylbenzene (PSDVB) particles are a suitable porous substrate for the removal of perfluorinated pollutants, as they are used in a variety of surface- and interaction-based applications, including separation technologies. In brief, several structural factors,

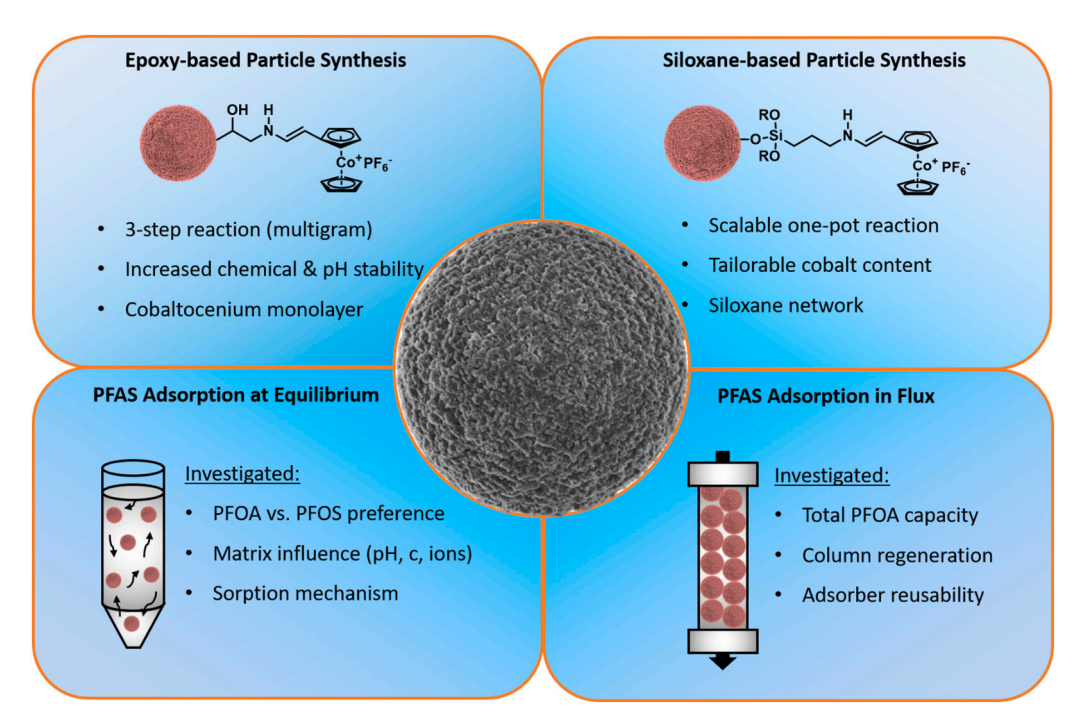


Fig. 1. Organisation and major outcomes of the present work.

such as (I) the size in the range of several  $\mu m$ , (II) the large surface area, and (III) the stability towards high pressures, are to be highlighted. The interfaces of such porous microparticles can be addressed chemically in a range of reactions. To demonstrate the viability of our approach, commercially available PSDVB particles were used as starting material for convenient functionalization strategies with cobaltocenium derivatives. The microparticles were either used directly or after the application of an epoxidization protocol. An overview of the used reactions is given in Fig. 2a + b. In the first attempt, oxidized precursor microparticles were used for cobaltocenium functionalization using a siloxane-based strategy [42].

### 3.1.1. Synthesis of siloxane-functionalized microparticles (PSDVB@APTES-Co)

Siloxane-functionalized stationary phases are widely used in a variety of analytical applications [43-45]. The ability to form a siloxane network on the interface is instrumental in trying to incorporate as much cobaltocenium as possible on the particle surface. In our preliminary work, we utilized the siloxane-based condensation of cobaltoceniumcontaining aminopropyl trimethoxy siloxane (CC-APTES) for particles' surface modification (Fig. 2a) [42]. We controlled the one-pot synthesis by adjusting the cobaltocenium content of the functionalized microparticle interface [42]. A summary is given to emphasize the simplicity of this procedure: The one-pot synthesis is performed by first synthesizing CC-APTES via a catalyst-free hydroamination reaction and later adding the particles for functionalization. Through this strategy, the surface properties could be tailored depending on the ratio of APTES to cobaltocenium or on the concentration of CC-APTES. After the reaction, the particles are separated from the reaction solution by either centrifugation or filtration and purified by a washing step. Thereby, we were able to obtain gram-scale batches of particles. The resulting particles were characterized by ATR-IR spectroscopy (ATR-IR), and the cobaltocenium content was verified by thermogravimetric analysis (TGA), energy dispersive X-ray spectroscopy (EDS), and inductively coupled plasma mass spectrometry (ICP-MS), and the structural integrity of the particles was validated by scanning electron microscopy (SEM). Within the present work, the siloxane-based approach for cobaltoceniumfunctionalized particles (PSDVB@APTES-Co) was prepared by utilizing a 1:1 molar ratio of APTES to ethynyl cobaltocenium hexafluorophosphate. In this way, no free amine functionalities were present. Furthermore, a 1:1 mass ratio of particle precursor to ethynyl cobaltocenium was found to be optimal for rapid functionalization and was, therefore, used for this work. For a more detailed description, the reader is referred to the experimental Section 2.3.2.

### 3.1.2. Epoxide-functionalized microparticle modification with cobaltocenium (PSDVB@epoxy-Co)

Next, an epoxy route was established to introduce the cobaltocenium moiety by an alternative and novel modification approach. This involves three steps (Fig. 2b): First, the PSDVB particles were treated with *meta*-chloro perbenzoic acid (mCPBA) to convert the residual double bonds to epoxides. In the next step, the epoxides were converted based on the nucleophilic ring-opening reaction of the epoxides with different secondary amines. To elucidate the efficiency of microparticles post-modification by this approach, a variety of amines ranging from linear ethyl-, butyl-, and hexylamine to sterically more demanding *tert*-butyl-, cyclohexyl-, ethanolamine, and aniline were tested. CHN analysis of the corresponding particles showed that after workup, the highest nitrogen content of 1.13 mass% was found for ethanolamine (Supporting Information, Table S1). Therefore, ethanolamine was chosen for all reactions presented herein.

By introducing an additional OH-group, the hydrophilicity should also be increased compared to the other amine alternatives, which will be beneficial for water-based separation technologies, as shown later. After successful amine addition, cobaltocenium was introduced via a catalyst-free hydroamination reaction [40,41]. A graphical representation is presented in Fig. 2c, highlighting the formation of the deep red cobaltocenium complex on the particle surface. As mentioned before, an excess of ethynyl cobaltocenium was used to guarantee efficient and full amine conversion.

During the stepwise approach, each step of the synthesis was monitored by FTIR spectroscopy. The resulting spectra are shown in Fig. 3a. After the initial epoxidation with *m*CPBA (red), a distinct new signal can be found at 1250 cm<sup>-1</sup>, which is attributed to the newly introduced epoxy group [46]. Due to the reaction with ethanolamine (blue), this sharp signal disappeared, and an efficient ring-opening reaction with the

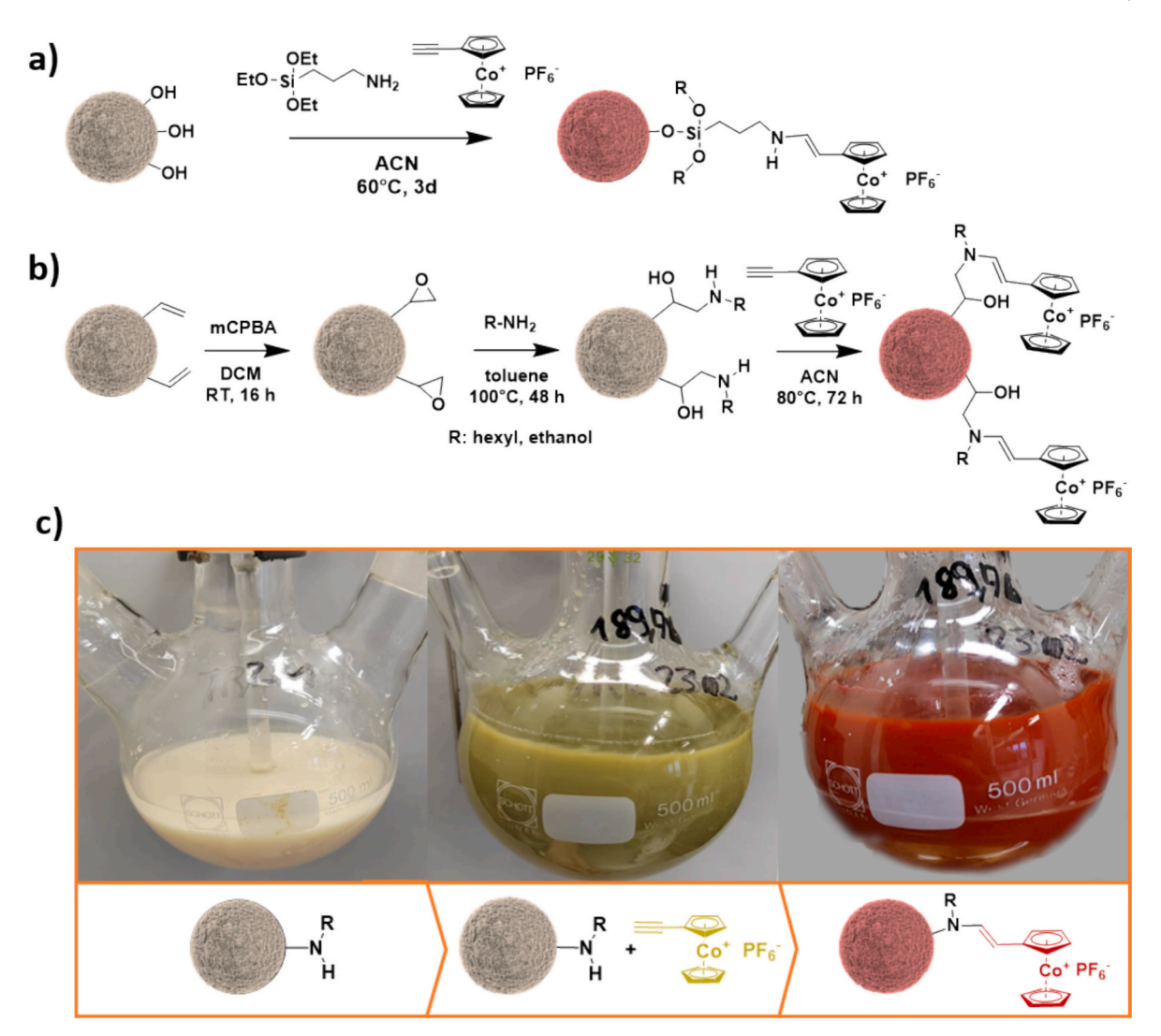


Fig. 2. Particle functionalization strategies for the introduction of cobaltocenium moieties to the microparticle surface; a) Siloxane-based approach in acetonitrile (ACN) according to the literature [42]; b) Epoxide-based approach by epoxidation in dichloromethane (DCM) using meta-chloro perbenzoic acid (mCPBA), amination in toluene, and cobaltocenium functionalization in ACN; c) Photographs of the different particle dispersion batches showing the color changes during cobaltocenium functionalization.

corresponding ethanolamine can be concluded. After the reaction of the aminated particles with ethynyl cobaltocenium hexafluorophosphate, the distinct  $PF_6$  signal at  $840~cm^{-1}$  and the cobaltocenium signal at  $557~cm^{-1}$  can be observed within the spectrum of the final product PSDVB@epoxy-Co~(purple). For comparison, the spectrum of the particles synthesized by the above-described siloxane condensation strategy (golden) featured very similar resonances for the cobaltocenium and  $PF_6$  region. Still, it showed an additional broad resonance in the range of  $1200-920~cm^{-1}$ , traditionally found for siloxane functionalized materials [47].

Next, thermogravimetric analysis (TGA) was utilized to characterize the synthesized material regarding the metallocene content. By controlled heating of the metallocene-modified materials in a nitrogen atmosphere, a ceramic material can be obtained at higher temperatures [48–51]. Depending on the overall composition, the residual weight is an indicator for the introduced metal-containing moieties and other inorganic components, for example, silicon. By comparing the siloxane (gold) and epoxy-functionalized (purple) microparticles, a clear trend became visible (Fig. 3b). Here, the siloxane-based particles show a higher residual mass of 21 mass% compared to the 15 mass% of the epoxy-based ones. This was expected since residual silica is most likely present due to the introduction of the silane network [52–55]. Since the

cobaltocenium is covalently attached, a successful functionalization could be verified this way. Furthermore, in both cases, cobalt-containing ceramic material is proposed, contributing to the overall ceramic yield. This is especially the case for PSDVB@epoxy-Co, where no siloxane was used. However, due to the complexity of the ceramic material formed [42], no further quantification was possible. Instead, the high ceramic yield in both cases was used to qualitatively verify the introduction of cobaltocenium via the siloxane and epoxy approach.

We obtained scanning electron micrographs to further evaluate the integrity of the microparticle structure (Fig. 3c). In both cases, the desired porous structure could still be found after the applied functionalization strategies. Furthermore, no broken or damaged microparticles were found, indicating suitable reaction conditions for preserving the particles' porous structure. EDS was performed for both particles to verify that cobaltocenium was present (Supporting Information, Fig. S4a + b). In both cases, cobalt could be found. For the siloxane-functionalized microparticles with cobaltocenium, a higher cobalt content of 0.78  $\pm$  0.13 mass% was determined, compared to the epoxy-functionalized ones with 0.27  $\pm$  0.15 mass%. These findings suggest a more efficient cobaltocenium modification using the described siloxane-functionalization protocol. However, since quantification is challenging with EDS, another analytical method for an adequate cobalt

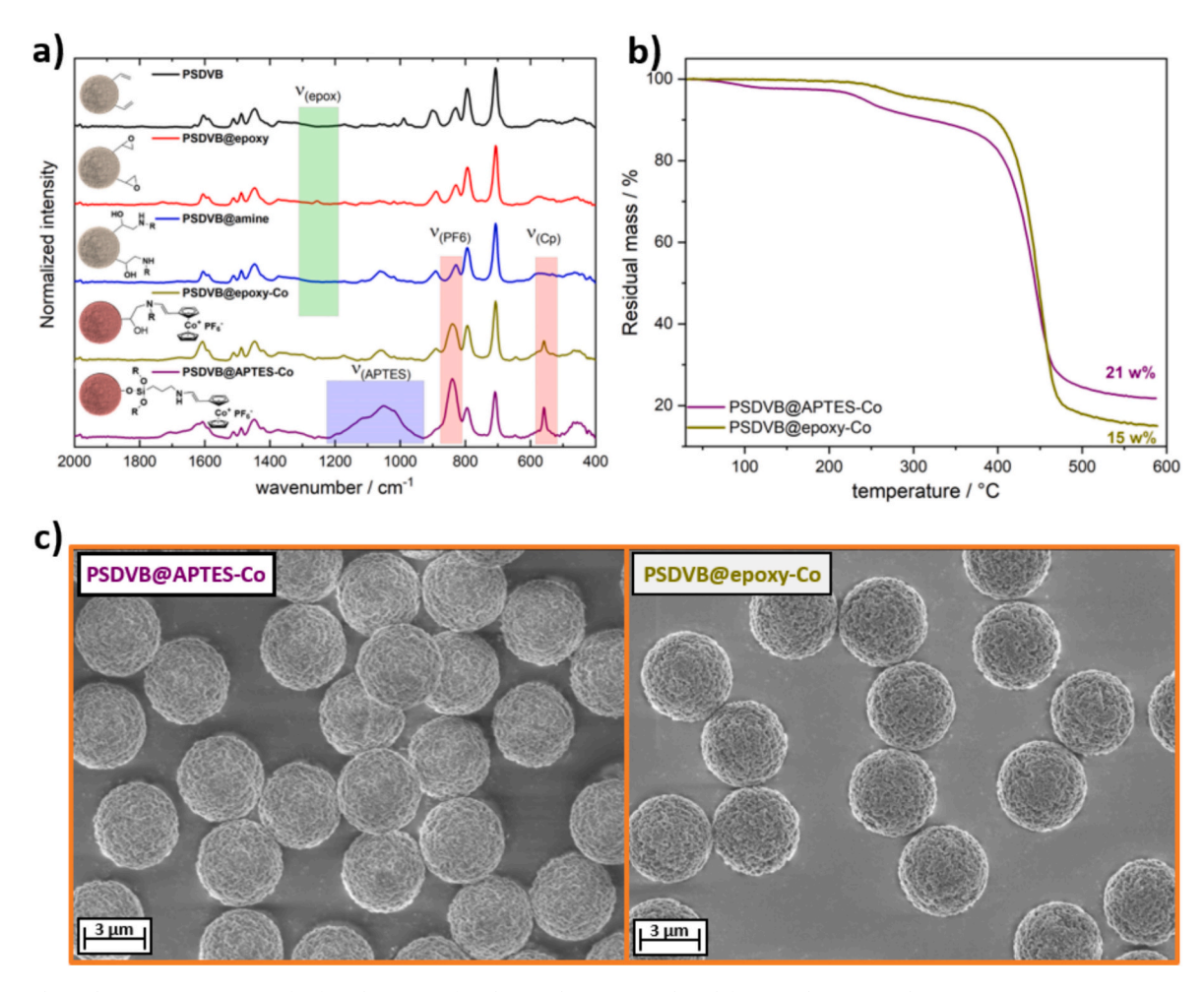


Fig. 3. Particle analysis; a) Comparison of infrared spectra of each step during epoxy-based functionalization, and PSDVB@APTES-Co in comparison; b) Thermogravimetric analysis of synthesized particles from 30 to 590 °C in a nitrogen atmosphere with a heating rate of 10 K min<sup>-1</sup>; c) Scanning electron micrographs of PSDVB@APTES-Co and PSDVB@epoxy-Co.

determination had to be carried out. Therefore, inductively coupled plasma mass spectroscopy (ICP-MS) was used.

In Table 2, the resulting cobalt contents are compiled for comparison. As expected, no cobalt content was found for the pure PSDVB particles. On the other hand, with both methods, a significant difference could be found for the siloxane- and epoxy-functionalized particles after cobaltocenium immobilization. Due to the siloxane network, PSDVB@APTES-Co presented the highest cobalt content with 10.83  $\mu g\,g^{-1}$  in ICP-MS. For PSDVB@epoxy-Co, where only a monolayer of cobaltocenium was introduced, 5.11  $\mu g\,g^{-1}$  was found, which is about half as much as with the other method. This trend agrees with the previous EDS data and the underlying functionalization mechanisms. The quantitative results obtained by ICP-MS indicate that the overall molar amount of cobalt could be determined, which will play a crucial role in understanding the adsorption mechanism at a later point. Since the adsorption processes depend strongly on surface interaction, the

Table 2
Summarized cobalt content measured by EDS or ICP-MS, and BET surface area.

Sample	Cobalt <sub>(EDS)</sub> (mass%)	Cobalt <sub>(ICP-</sub> MS) (mass%)	n <sub>Cobalt</sub> (μmol mg <sup>-1</sup> )	BET- Surface (m <sup>2</sup> g <sup>-1</sup> )	ρ <sub>Cobalt</sub> (μmol m <sup>-2</sup> )
PSDVB	nd	0.00	~0	369	~0
PSDVB@APTES-	0.78 $\pm$	1.08 $\pm$	0.18	84	2.14
Co	0.13	0.01			
PSDVB@epoxy-	$0.27~\pm$	$0.51~\pm$	0.09	233	0.39
Co	0.15	0.01			

addressable surface was analyzed using nitrogen gas adsorption (Supporting Information, Fig. S2).

Compared to the starting materials, the surface area was reduced by siloxane-functionalization (PSDVB@APTES-Co). This is due to the formation of the siloxane network at the particles' surface, which is assumed to occupy and seal the cavities of the micropores first. In contrast to PSDVB@APTES-Co, a larger surface area was found for the PSDVB@epoxy-Co, which was only capable of forming a single surface layer upon functionalization. Furthermore, the grafting density  $\rho$  could be calculated from the surface area and the molar amount of introduced cobalt per gram particle (Table 2). Here, the siloxane network of PSDVB@APTES-Co presented a significantly higher grafting density of cobaltocenium of 2.14  $\mu$ mol m $^{-2}$  compared to the monolayer functionalization of PSDVB@epoxy-Co with 0.39  $\mu$ mol m $^{-2}$ .

In summary, the successful microparticle modification with two different architectures was validated, and the prepared particles could be investigated in model PFAS adsorption studies, as described in the following sections.

### 3.2. Adsorption and analysis of model PFAS at equilibrium

Following the successful functionalization, the respective particle charges were analyzed regarding the adsorption of the model PFAS, namely PFOS and PFOA. By studying the adsorption at sorption equilibrium, crucial influences on the interaction between the analyte and the material and the adsorption mechanism can be obtained, which are important for further investigations in flow. A visual representation of

the workflow is given in Fig. 4.

A distinct amount of particles (0.1 mg mL $^{-1}$ ) was introduced to a spiked solution (50 mL) with either PFOA or PFOS and incubated for 24 h at 25 °C in a shaking device (600 RPM). After centrifugation and removal of the particles, the solution was spiked with the respective  $^{13}\text{C}$  enriched standard for PFOS or PFOA quantification. The solution was purified and reduced by filtration over a SPE (WAX-phase), followed by elution with MeOH and ammoniacal MeOH. After evaporating, the sample solution was adjusted to a 50/50 MeOH/H $_2$ O mixture with a corresponding volume of 1 mL, which was used for analysis. For a more detailed description, the reader is guided towards the corresponding section in the material and methods part (see Section 2.4.1.1).

### 3.2.1. Quantifying the adsorption efficiency

The ratio of the standardized peak areas of the complex sample and the corresponding  $^{13}\text{C}$  reference determined the sorption efficiency. As the values for the respective PFOS and PFOA adsorption were generally found to be very high (up to >90 %), so-called  $K_d\text{-}\text{values}$ , given by the quotient between mass concentrations in the sorbents and the solutions at equilibrium, were used for a better comparison of the acquired data. Such values are commonly used in sorption measurements to quantify the sorption efficiencies of clays [56]. The scale of sorption values is thereby expanded, and differences in otherwise very similar sorption efficiencies SE can then be shown more clearly. The sorption efficiency SE can be used to calculate the complex formation constant  $K_d$ :

$$SE = \frac{m_{GG}}{m_{initial}} \times 100\% \tag{1}$$

$$K_d = \frac{m_{sorbed} \times V_{sample}}{m_{GG} \times m_{adsorbent}} \tag{2}$$

where

 $m_{GG}$  mass in the liquid,  $m_{sorbed}$  mass on the solid phase,  $m_{initial}$  total mass before sorption,  $m_{adsorbent}$  mass of the solid (particles), and  $V_{sample}$  volume of the liquid phase.

The results of the initial experiments are given in Fig. 5a. Here, both modified microparticle batches were compared regarding the sorptive character of PFOS and PFOA for a given spike amount. In both cases, high adsorption of both compounds could be found, and preferences could be shown depending on the material. In the case of PSDVB@APTES-Co, the sorption of PFOS was favored over PFOA. For PSDVB@epoxy-Co, higher overall adsorption and a reverse preference from PFOS to PFOA could be noticed. These results imply that the

functionalization strategy (siloxane or epoxide-based) affects the resulting sorption behavior more than expected.

### 3.2.2. Influence of the matrix and surrounding counter ions

Next, the influence of the matrix was analyzed since most realistic separation applications for PFAS removal occur in environments containing salts. To investigate the effect of different matrices on the adsorption behavior, PSDVB@APTES-Co and PSDVB@epoxy-Co microparticle batches were tested in Milli-Q water/ACN (95/5 by volume) and Evian (bottled) water/ACN (95/5 by volume; see Section 2.4.2.1). In our case, Evian water was used as a model matrix due to its strictly controlled pH and ion composition (Supporting Information, Table S2) and wide commercial availability. For detailed verification, the samples were tested as triplicates. The resulting adsorption and K<sub>d</sub>-values were compiled in Fig. 5b. Based on our data, we concluded that the matrix has a distinctive effect on the PFOS and PFOA adsorption. For PSDVB@APTES-Co, an increased tendency towards adsorption of PFOS was found, indicating an interaction-based preference. Normally, one would expect a slight decrease in adsorption in the presence of an ionic matrix due to comitative interaction with other anions [57]. This way, the material preference between PFOA and PFOS in the presence of a matrix was influenced: For PSDVB@epoxy-Co, a preference inversion from a higher tendency to adsorb PFOA in pure water to a preference for PFOS in an ionic matrix was found. Here, chloride can especially influence the adsorption of PFOA for common PFAS adsorbents [25,57]. On the other hand, it was reported that divalent cations can increase the hydrophobicity of the perfluorinated compounds to a certain degree, which is beneficial for the hydrophobic cobaltocenium hexafluorophosphate (PF<sub>6</sub>) surface [58,59]. In our specific case, ion exchange of PF<sub>6</sub> to other hydrophilic anions like chloride or hydroxide is difficult to achieve. It is, if necessary, generally done before forming the ion exchange material [60-62]. Incorporating perfluorinated compounds into the matrix leverages their beneficial cationic effects and enhanced hydrophobic affinity, while any adverse competitive interactions remain negligible. This increased hydrophobicity, together with the presence of additional cations, may also promote the stabilization of multilayer BET-type adsorption, ultimately resulting in enhanced overall adsorption.

The introduction of an ionic matrix positively influenced the sorption capacity, further highlighting the oleophobic behavior of PFAS in the presence of various inorganic ions. These findings demonstrate the potential of the synthesized material for general drinking water purification applications.

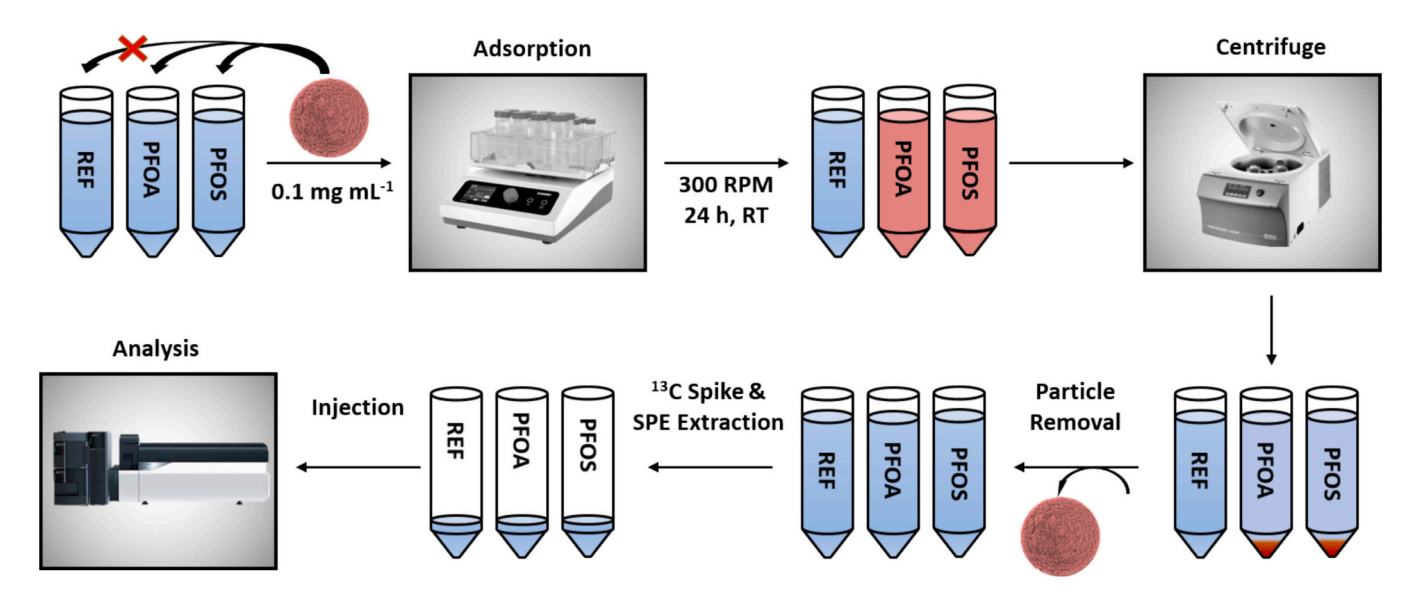


Fig. 4. Workflow for PFOS and PFOA adsorption analysis at equilibrium.

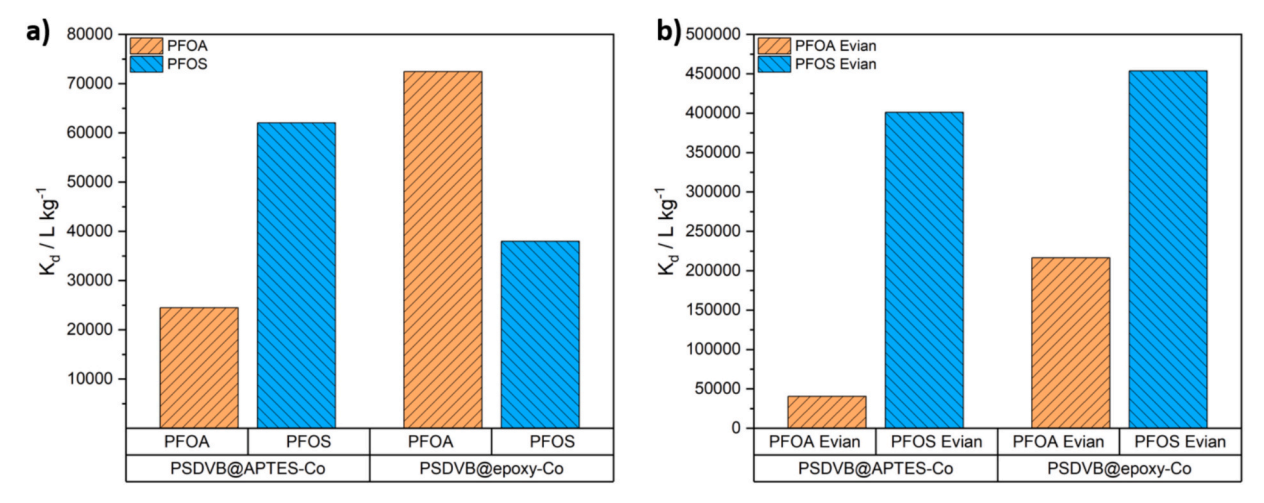


Fig. 5.  $K_d$  values of tested materials PSDVB@APTES-Co and PSDVB@epoxy-Co in different matrices; a)  $K_d$  determination of in 95/5 Milli-Q water/ACN b)  $K_d$  determination in commercially available Evian water.

### 3.2.3. Influence of the pH value on the PFOS and PFOA adsorption and the microparticles' stability

Besides matrix effects, the influence of varying pH values on the adsorption efficiency was investigated. For this purpose, samples with a given spike amount of perfluorinated analyte were tested at pH values ranging from 0 to 14, that is, at pH values of 0, 2, 4, 6, 8, 10, 12, and 14. The results for the two different materials on the  $K_d$ -values are given in Fig. 6.

In both cases, the results show that the best adsorption rates occur at the physiological pH range of pH 6 to pH 8. For PSDVB@APTES-Co (Fig. 6a), the K<sub>d</sub>-values decreased at higher pH values as the complex was no longer able to adsorb both model PFAS. The effect could be observed by the change from pH 8 to 10. At a pH value of below 6-8, both analytes, but preferably PFOS, were adsorbed. In contrast, at pH 10, both K<sub>d</sub>-values significantly decreased. This might be caused by the disintegration of the siloxane network and the resulting detachment of cobaltocenium at higher pH [63]. For acidic pH values, the adsorption was also reduced, but instead of chemical stability, ionic interactions may be the main reason, as the perfluorinated acids get increasingly protonated [64]. In comparison, for PSDVB@epoxy-Co, where the cobaltocenium motive is attached via the opening of an epoxide, the influence of pH was less pronounced. Again, optimal adsorption was found at physiological pH values, but a decrease was determined for both the highest and the lowest pH values. Additionally, a slight preference towards PFOA was found at a lower pH and for PFOS at a higher pH.

### 3.2.4. Influence of PFOS and PFOA concentrations and determination of the adsorption mechanism and isotherms

In the next step, adsorption isotherms were investigated to gain additional information on the adsorption mechanism and process of the herein-prepared materials. The effect of different concentrations of PFOS and PFOA on the adsorption rates and the resulting  $K_d$ -values were measured for the two materials PSDVB@APTES-Co and PSDVB@epoxy-Co (Fig. 7).

The results showed a general increase in  $K_d$  with increasing analyte concentration resulting in higher equilibrium-concentrations  $\beta_{GG}$  as:

$$\beta_{initial} = \beta_{GG} + \beta_{sorbed} \tag{3}$$

The concentration  $\beta_{sorbed}$  is used to calculate  $m_{sorbed}$  and thus the coverage q:

$$q = \frac{m_{\text{sorbed}}}{m_{\text{adsorbent}}} \tag{4}$$

Plotting the coverage q versus  $\beta_{\text{GG}}$  gives the adsorption isotherms (Fig. 8).

A large variety of different adsorption isotherms are known in the literature, describing the interaction of solutes or gaseous species with

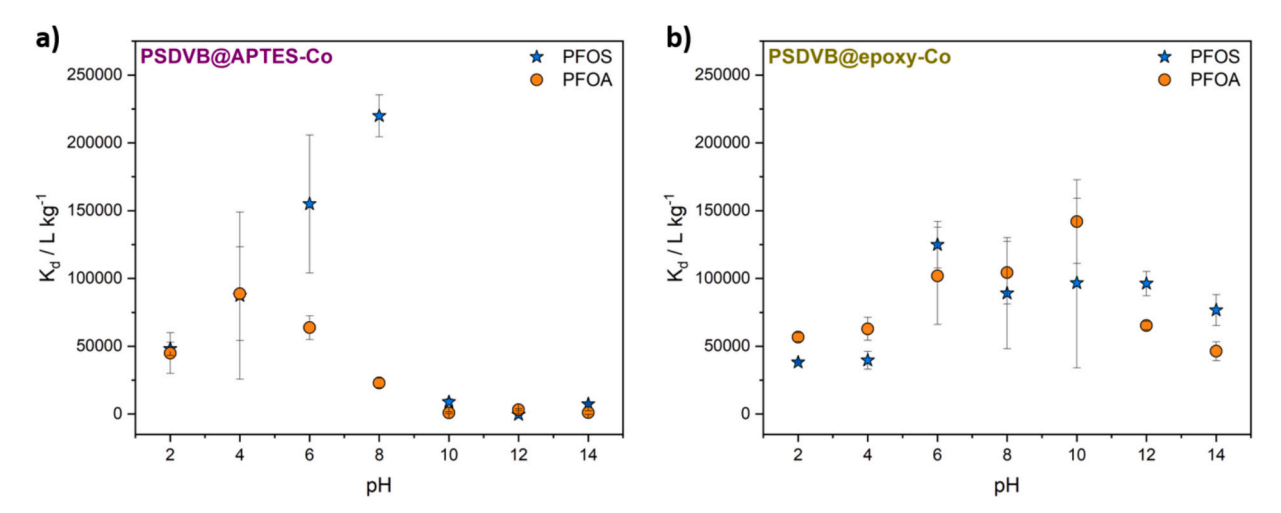


Fig. 6. Effect of the pH-value on the  $K_d$ -value of PFOA and PFOS in an average over three samples; a) pH effect on  $K_d$ -value of PSDVB@APTES-Co; b) pH effect on  $K_d$ -value of PSDVB@epoxy-Co.

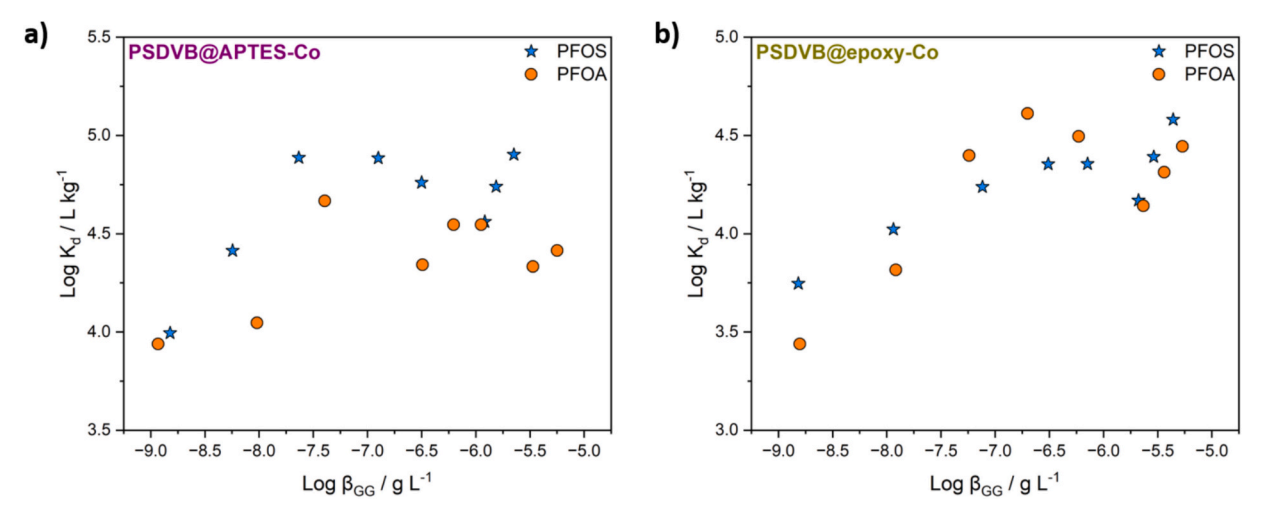


Fig. 7. Effect of the concentration on the  $K_d$ -value of PFOA and PFOS plotted as Log  $K_d$  vs equilibrium concentration  $\beta_{GG}$ ; a) Concentration effect on  $K_d$ -value of PSDVB@APTES-Co; b) Concentration effect on  $K_d$ -value of PSDVB@epoxy-Co.

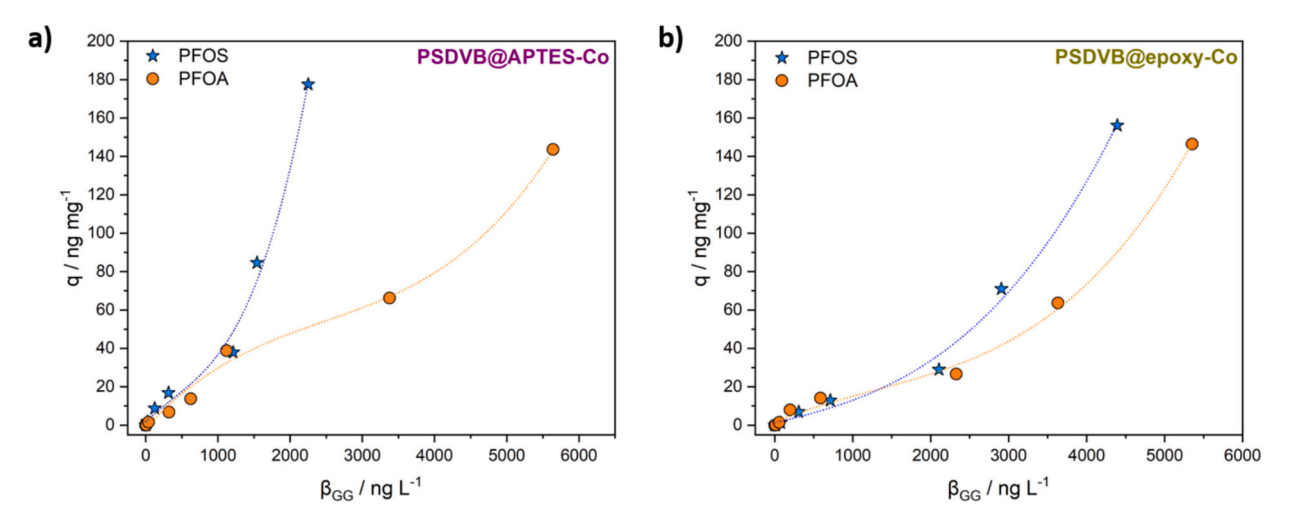


Fig. 8. Adsorption isotherms for a) PSDVB@APTES-Co and b) PSDVB@epoxy-Co for PFOA and PFOS at 25 °C.

solids [56,65-67]. With varying equilibrium concentrations in gases or liquids, different courses of the adsorption isotherms were generally found, which may be attributed to different adsorption mechanisms. The examples range from linear relationships between loads and equilibrium concentrations, mostly found for very low concentrations (Henry), to more or less concavely rising curves matched with exponential terms (Freundlich), and to systems where a kind of saturation plateau is attained as described in the Langmuir isotherm. Finally, Brunauer-Emmett-Teller (BET) isotherms show continued adsorption beyond initial saturation, indicating multilayer formation on the solid surface [68,69]. In our case, all curves in Fig. 8 can best be described with the BET theory with a very small intermediate saturation window. Within the framework of this theory, the course of the curve changes more than with other adsorption mechanisms (Langmuir, Temkin, Freundlich, Henry), which either have a linear increase of the coverage (Henry) or get close to a maximum. Additional information on the calculation of the BET and comparison to the discussed mechanisms can be found in the Supporting Information Section 5.

The obtained result also matches the development of the  $K_d$ -values with increasing concentrations, where, according to BET theory, a multilayer adsorption process occurs. An overview of our proposed interactions can be concluded from Fig. 9. Here, three kinds of interactions are proposed to play a major role in PFAS adsorption, namely (I) ionic

interactions, (II) hydrophobic interactions, and (III) secondary structure-based and further F-F interactions. Whereas the first adsorption layer is formed by strong ionic and weaker aromatic interactions, secondary layers may be formed by F-F-interactions and further structural factors. The surface modification process, which is intricate for the adsorption of perfluoroalkyl substances (PFAS), involves the introduction of a cationic nature through the incorporation of cationic, hydrophobic, and aromatic cobaltocenium fluorophosphate. The investigation revealed that both siloxane and epoxy modifications are suitable for this purpose, and the hydrophobic PSDVB particle can be modified to enhance its affinity for PFAS, accompanied by a slight decrease in the addressable surface area. Although a slight decrease in porosity is expected, the surface charge on the particle, and the macroporous structure lead to an adsorption beyond ionic pairing but rather in the development of secondary layering of PFOS and PFOA and increased adsorption. This effect is further increased in the presence of an ionic matrix.

### 3.3. PFOA analysis in flow

With insights into the adsorption mechanism under equilibrium conditions, the viability of an application in flow will be investigated in the following. The first step was to develop a flow-based method using

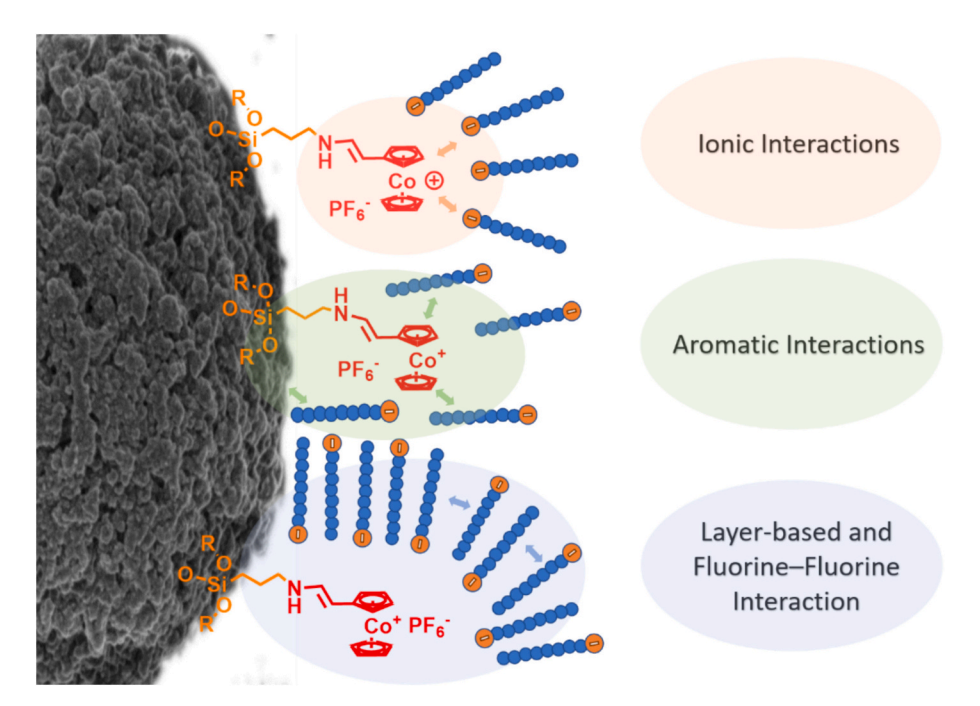


Fig. 9. Proposed interactions of PFAS and the cobaltocenium-functionalized porous particle: Initial ionic and aromatic interactions create an environment on the particle surface, where layer-based adsorption beyond ion-pairing is possible.

the synthesized material as a stationary phase. The overall capacities, as well as regeneration and reuse, were investigated in more detail.

An overview of the setup used is shown in Fig. 10a. For means of volume transport, a conventional HPLC pump was used, which was supplied from a spiked feed, allowing a controlled and continuous flow of 2 mL min<sup>-1</sup>. The experimental column consisted of 100 mg of modified microparticles and was connected to the pump outlet. Further details and images of the column and packing can be found in Supporting Information Fig. S1. A single column was prepared for each measurement, except for the reusability studies, as described later. During the experiments, samples were collected in weighed vessels, the exact volumes were determined by weight, and LC-MS or IC were used to measure the analyte concentrations. In cases where subsequent elution was performed, the column was suspended and manually rinsed with air and PFAS-free eluent (Fig. 10b). After that, PFOA was eluted via a syringe pump at a flow rate of 1 mL min<sup>-1</sup> with a defined amount of ammoniacal MeOH (0.1 vol% conc. NH<sub>3</sub>) according to DIN EN 17892:2024-08 (Ref. [70]) or with ionic MeOH (1 mass% sodium chloride).

### 3.3.1. Total PFOA capacity

After we demonstrated the feasibility in a low concentration regime of 20  $\mu g \; L^{-1}$ , which can only be directly detected by LC-MS, the next objective was to verify our findings utilizing a different method and concentration range. At higher concentration ranges (2–500 mg  $L^{-1}$ ), several crucial material properties, like the total adsorptive capacity, played a major role. In this regard, we selected ion chromatography (IC) as an established detection method for perfluorinated substances [71]. Based on this method, we were able to analyze the PFOA concentration before [41]. Within the present study, we focused on the less-adsorbing substance PFOA, as it is capable of indicating the critical threshold points for our process. In addition, the procedure was significantly more accurate with only one analyte, as interactions between the analytes were prevented.

One of the most important characteristics of adsorption media is the total capacity of the adsorbed analyte. To investigate our particles, the

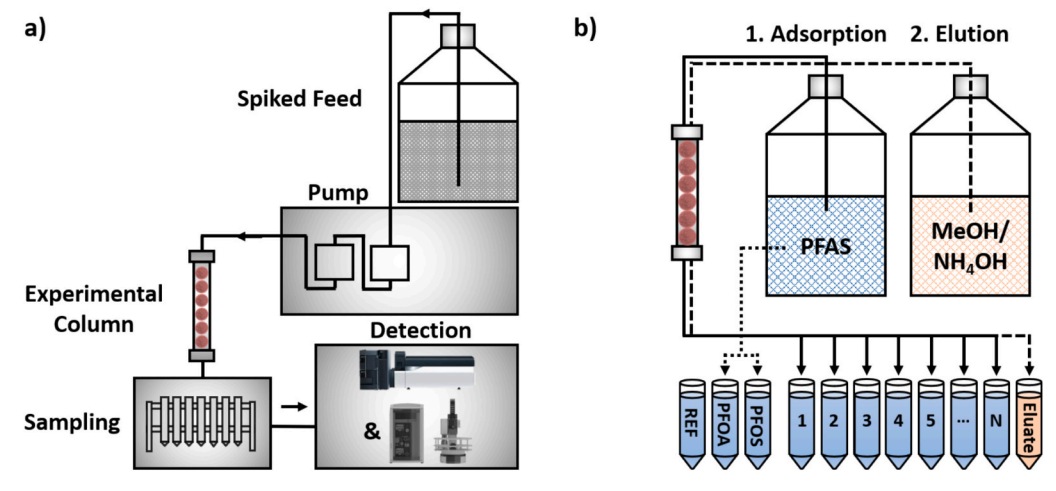


Fig. 10. Overview of setup and workflow for PFOA experiments in flow.

packed columns were treated with a highly concentrated PFOA solution (500 mg  $\rm L^{-1}$ ), and the resulting concentration of the samples was determined (Fig. 11).

The adsorption can be calculated via the ratio of concentration between the feed and the sample. The accumulated adsorbed moles of PFOA were used to calculate the total capacity  $S_{PFOA, mg}$  (Section 2.4.2.1), making a comparison of the functionalized materials possible (Table 3). Every measurement was at least performed as a duplicate.

In addition to the functionalized particles, the starting material was also characterized. Here, an adsorption capacity of  $55.2 \pm 0.3~\mu g~mg^{-1}$  was found. By introducing cobaltocenium to the microparticle structure, the capacity could be increased by a factor of 3.9 for PSDVB@APTES-Co and a factor of 5.3 for PSDVB@epoxy-Co. Here, the siloxane as well as the epoxy approach have proven successful. At first glance, PSDVB@APTES-Co provided a lower capacity of  $215 \pm 0.6~\mu g~mg^{-1}$  compared to the  $292.9 \pm 3.3~\mu g~mg^{-1}$  of PSDVB@epoxy-Co. By dividing the  $S_{PFOA,mg}$  by the molar amount of cobaltocenium attached on the respective particle batch, a ratio  $N_{PFOA,\ Cobalt}$  of PFOA molecules adsorbed per cobaltocenium unit ( $n_{Cobalt}$ ,  $s_{ample}$ ) can be calculated. To incorporate only the effect of the cobaltocenium, the adsorption based on the raw particle  $S_{PFOA,PSDVB}$  was subtracted.

$$N_{PFOA,Cobalt} = \frac{S_{PFOA,sample} - S_{PFOA,PSDVB}}{n_{Cobalt,sample}}$$
(5)

In both cases, the resulting number is higher than otherwise expected in a pure ion exchange-based process. The higher values correlate well with the previously collected adsorption data at equilibrium and further strengthen the idea of a BET-type adsorption mechanism. Furthermore, the lower ratio of 2.1 for PSDVB@APTES-Co compared to 6.5 for PSDVB@epoxy-Co shows that although the siloxane network allows a lot of cobaltocenium to be introduced, the surface area is significantly reduced. This reduces the effectiveness of the formation of secondary structures that promote adsorption.

To calculate the effect of the particle surface on the PFOA adsorption capability, the available surface area per gram  $A_{BET,\;particle}$  was taken into account (Table 1), and the specific surface capacity  $A_{PFOA}$  could be calculated.

$$A_{PFOA,} = \frac{S_{PFOA,mg} \bullet 1000}{A_{BET,particle}} \tag{6}$$

By comparing the obtained  $A_{PFOA}$  values before and after functionalization, the trend is even more visible: The specific surface capacity is increased compared to the unfunctionalized particle by 1727 % in the case of PSDVB@APTES-Co and about 833 % by PSDVB@epoxy-Co. To correlate this surface enhancement directly to the cobaltocenium

**Table 3**Summarized material properties.

Sample	S <sub>PFOA</sub> , mg (µg mg 1)	N <sub>PFOA</sub> , Cobalt	A <sub>PFOA</sub> <sup>c</sup> (μmol m <sup>-2</sup> )	ΔA <sub>PFOA</sub> <sup>d</sup> (%)	$I_{A,Cobalt}^e$ (µmol m $^{-2}$ )/ (µmol m $g^{-1}$ )
PSDVB	$55.2 \pm 0.3$	0	0.36	1	
PSDVB@APTES- Co	$\begin{array}{c} 215.4 \\ \pm \ 0.6 \end{array}$	2.1	6.21	1727	33.8
PSDVB@epoxy- Co	$\begin{array}{c} 292.9 \\ \pm \ 3.3 \end{array}$	6.5	3.00	833	34.6

- <sup>a</sup> Total PFOA sorption capacity S.
- b Molar ratio of PFOA adopted per cobaltocenium unit.
- <sup>c</sup> Specific PFOA surface capacity.
- <sup>d</sup> Difference in specific surface capacity compared to PSDVB in %.
- <sup>e</sup> Impact factor to describe the influence of cobaltocenium on the surface enhancement.

amount  $n_{Cobalt,mg}$ , an index  $I_{A,cobalt}$  can be calculated:

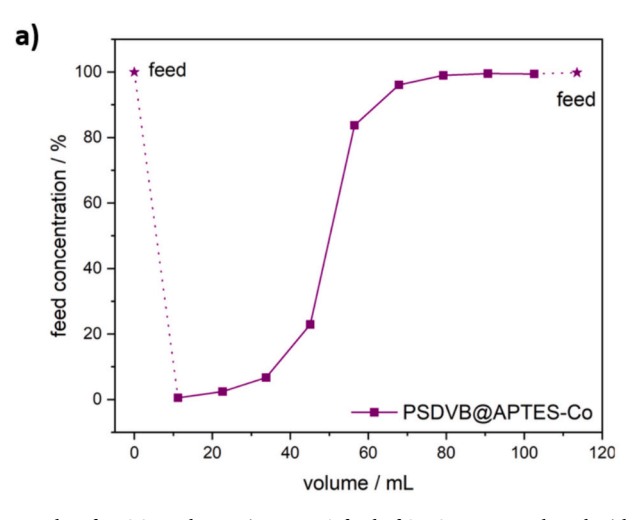
$$I_{A,Cobalt} = \frac{A_{PFOA,}}{n_{Cobalt.mg}} \tag{7}$$

Here, a very similar value of  $\sim$ 34 in both cases shows the comparable correlation and the direct influence of the introduced cobaltocene on the surface capacity.

### 3.3.2. Regeneration and reusability

To simulate the low environmental concentrations, adsorption at low PFOS and PFOA concentrations of 20  $\mu g \ L^{-1}$  in the feed was performed next. This ensured that the total possible adsorbed amount of PFOA is always below the sorption capacity, and predominantly, the elution and reusability can be evaluated. The results are presented in Fig. 12. For the siloxane-functionalized metallopolymer material PSDVB@APTES-Co, the measurements (Fig. 12a) showed promising results.

In general, the adsorption of PFOA and PFOS was nearly complete (>98 %) for the eight samples. After elution with ammoniacal methanol, almost a quantitative desorption and a target concentration very close to the expected total value were found for PFOA. For the counterpart PFOS, a slightly higher value than expected was obtained. This may be due to the experimental design and the generally difficult handling of the perflorinated tensides. In comparison, a similar adsorption behavior for both components was also found for PSDVB@epoxy-Co (Fig. 12b). This time, the concentrations obtained after elution were slightly different from the expected values, indicating that the elution conditions were not yet optimal. However, these first experiments demonstrated the



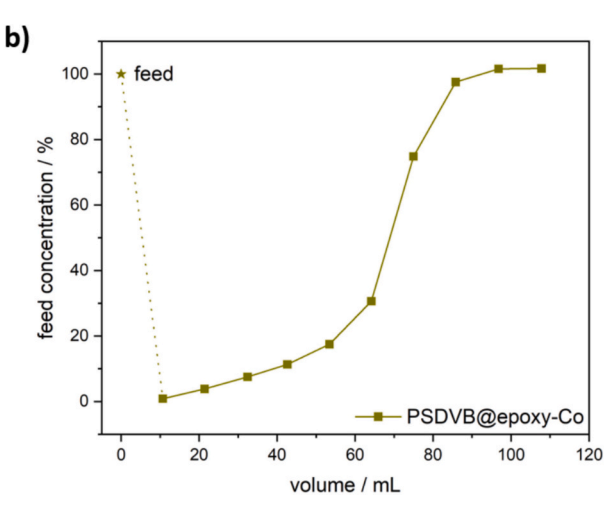


Fig. 11. Results of PFOA total capacity tests. A feed of 97/3 water/methanol with a concentration of PFOA of 500 mg L<sup>-1</sup>, a flow rate of 2 mL min<sup>-1</sup>, and sampling every 5 min were used. a) Adsorption profile for PSDVB@APTES-Co; b) Adsorption profile for PSDVB@epoxy-Co.

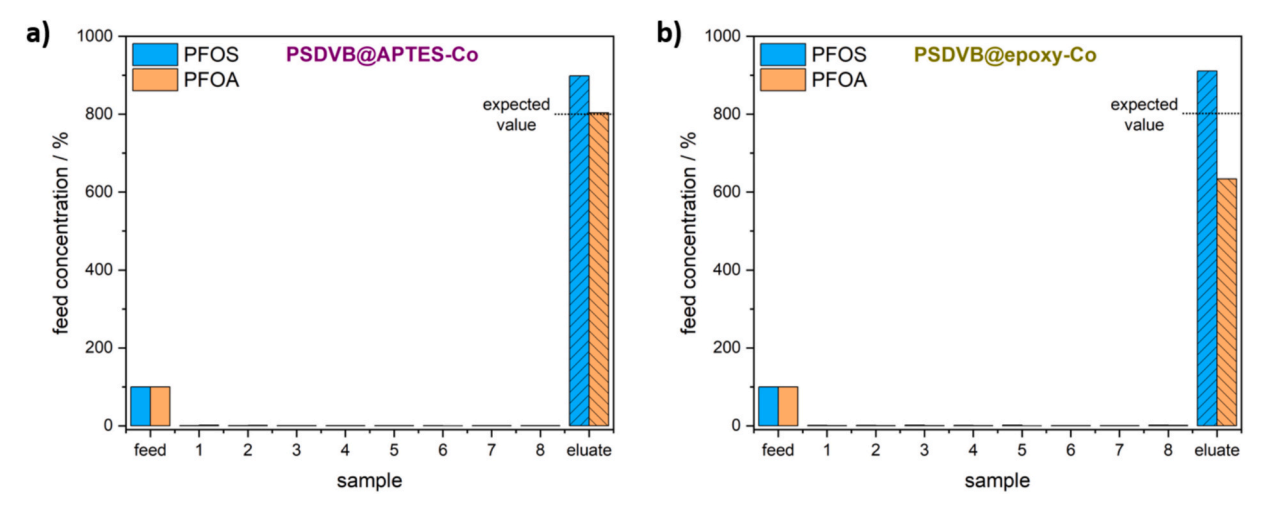


Fig. 12. Results of model PFAS adsorption and controlled desorption test with an experimental column, a feed of 95/5 water/ACN with a concentration of PFOA or PFOS with 20  $\mu$ g L $^{-1}$ , a flow rate of 2 mL min $^{-1}$ , sampling every 10 mL, and elution with 5 mL methanol and 5 mL ammoniacal methanol. The experiment is performed by first measuring the analyte concentration in the feed, followed by eight-column samples with equal volumes, and analyzing the concentration after elution. The concentrations are given as a fraction of the initial analyte concentration in the feed: a) PFOA and PFOS concentrations compared for the respective column experiment using PSDVB@epoxy-Co.

feasibility of efficient PFOA and PFOS capture in flow and with limited exposure time ( $2~\mathrm{mL\,min}^{-1}$ ) compared to previous studies. Furthermore, the elution worked at an acceptable level to concentrate the recovered perfluorinated substances further. By balancing these cycles, continuous purification should be possible.

To further investigate the adsorption process, reusability, and recovery of PFOA, repeated experiments with the same experimental columns were performed. As we only have a setup with one pump available, no gradient method or direct eluent shift could be performed. Instead, elution was carried out using a syringe pump after brief rinsing, as described above. The synthesized materials were characterized in terms of reusability in five cycles each. Each cycle consisted of (I) checking the feed concentration, (II) four samples of column-adsorption purification, and (III) elution and detection of the desorbed PFOA. Additionally, the elution was carried out in two different ways: by ammoniacal methanol or ionic methanol.

As indicated by the previously obtained data for low concentrations (of 20  $\mu$ g L<sup>-1</sup>), the reusability and PFOA elution could be demonstrated (Fig. 13). When ammoniacal methanol was used for elution, according to DIN EN 17892:2024-08, [70], in both cases, a similar trend was found: The first desorption cycle resulted in a higher PFOA concentration of 460 % than the expected 400 %. This might be caused by impurities removed by the alkaline conditions that interfere with the measurement. The following cycles result in very similar desorption of 319  $\pm$  60 % for PSDVB@APTES-Co and 314  $\pm$  44 % for PSDVB@epoxy-Co. In comparison to the siloxane-based particles, while measuring the column adsorption of PSDVB@epoxy-Co (Fig. 10b), after the second cycle, a sudden increase in the residue of PFOA can be found. This is most likely not attributed to the sorption capacity but rather to a different matter. We assume that the change in pressure during the detachment of the column disrupted the particle packing, leading to cracks and enabling by-flow. Further validating this idea is the reduced concentration found in run 4 and the sudden increase in run 5. If the reason was based on the material properties, a linear trend would be expected instead. However, overall, this effect can be solved by using a sophisticated packing procedure.

When ionic methanol was used for elution, better results regarding reusability and reproducibility were found (Fig. 10c+d). Here, PFOA concentrations of  $350\pm16$ % for PSDVB@APTES-Co and  $329\pm22$ % for PSDVB@epoxy-Co were obtained. Furthermore, only a slight disturbance of the column material was found for PSDVB@APTES-Co in run 3 and run 5 (Fig. 10c). For PSDVB@epoxy-Co, quantitative

adsorption during the column adsorption was found (Fig. 10d). Generally, the elution with ionic methanol produced better results overall. Furthermore, by not using ammonia, the physiological pH should be better for long-term column stability, especially for the siloxane-based particles, as discussed earlier.

### 3.3.3. Performance comparison to commercially available ion exchange resins

Because of the high environmental relevance of PFAS, it is an asset to compare the newly obtained data to standardized materials. Most recently, a series of structurally very similar and commercially available high-performance ionic resins, namely Purolite® A600E, A520E, and A532E, were investigated regarding PFAS adsorption [72]. Instead of the cationic cobaltocenium unit, these resins are modified by widely used tertiary amines of various kinds. By this total PFOA capacities of respectively 125.2  $\mu g \ m g^{-1}$ , 134.7  $\mu g \ m g^{-1}$ , and 142.1  $\mu g \ m g^{-1}$  were obtained, which is, as expected, better in comparison to the unmodified PSDVB-particles (55.2  $\mu g \ m g^{-1}$ ) but significantly worse compared to PSDVB@APTES-Co with 215.4  $\mu g \ m g^{-1}$  and PSDVB@epoxy-Co with 292.9  $\mu g \ m g^{-1}$ . Furthermore, regeneration was only possible by undesired dilute NH<sub>4</sub>Cl or NH<sub>4</sub>OH solutions, in comparison to our elution containing methanolic NaCl.

### 3.3.4. Recycling/upcycling of the column material

As a final step, SEM analysis was performed on the particles after the column experiments to assess their morphological stability and confirm reusability. This evaluated the overall integrity of the particle during column preparation and after the adsorption experiment. As can be seen in Supporting Information, Fig. S4c + d, the particles were not altered in this process. Furthermore, the adsorption of perfluorinated pollutants onto the particular substrate could be shown via EDS by an increase in overall fluorine content compared to the initial functionalized particle. Whereas a lower fluorine content of 2.1 mass% and 0.8 mass% was found for the respective particles before the capacity experiment, a drastic increase to 4.2 mass% for PSDVB@APTES-Co and 2.4 mass% for PSDVB@epoxy-Co were found. Because of the high vacuum required to prepare SEM samples, these values should not be used for quantification. This way, a large portion of the volatile PFOA may be evaporated. Nevertheless, the remaining PFOA demonstrates the sorption capabilities of the material in combination with structural integrity throughout the sorption process.

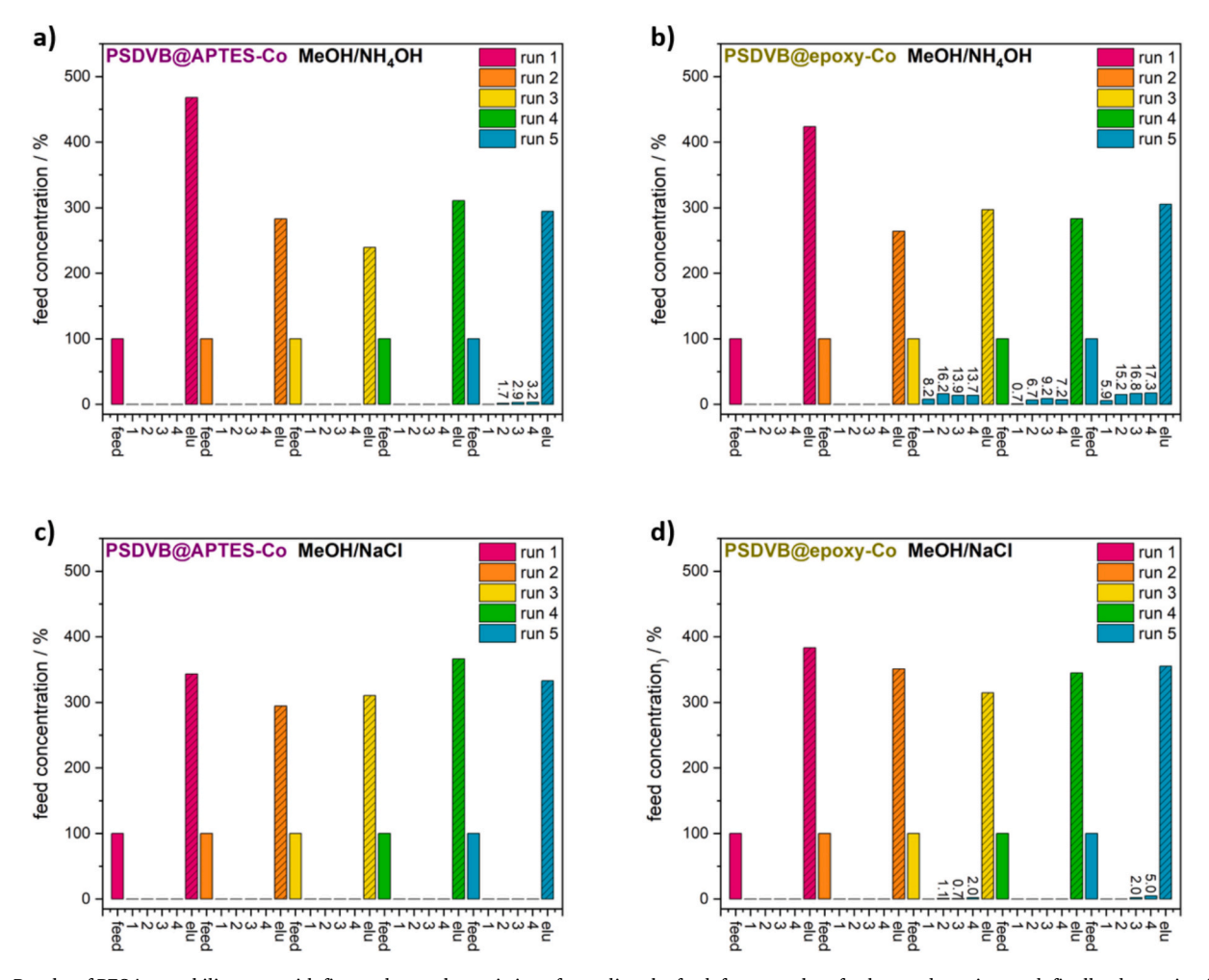


Fig. 13. Results of PFOA reusability tests with five cycles, each consisting of sampling the feed, four samples of column adsorption, and, finally, desorption from the column. A feed of 97/3 water/methanol with a concentration of 2.25 mg L $^{-1}$  PFOA, a flow rate of 2 mL min $^{-1}$ , sampling every 2.5 min, and elution with 5 mL of either ammoniacal methanol or ionic methanol at a flow rate of 1 mL min $^{-1}$ . The repeated experiment is performed by first measuring the analyte concentration in the feed, followed by four column samples with equal volumes, and analyzing the concentration after elution. The concentrations are given as a fraction of the initial analyte concentration in the feed. The experiment is repeated five times with the same column and elution method: a) PFOA concentrations compared for each subsequent column experiment of PSDVB@APTES-Co and ammoniacal methanol elution; c) PFOA concentrations compared for each subsequent column experiment of PSDVB@APTES-Co and ionic methanol elution; d) PFOA concentrations compared for each subsequent column experiment of PSDVB@epoxy-Co and ionic methanol elution.

### 4. Conclusions

In PFAS removal, one of the biggest challenges for new adsorbent material is to combine high adsorption capacity and excellent regeneration capabilities. In recent years, cobaltocenium-containing material has attracted significant attention due to its promising potential in this regard. In this work, we presented two different ways to functionalize commercially available PSDVB particles with cobaltocenium. This was done either in a one-pot reaction by siloxane condensation (PSDVB@APTES-Co) or by ring opening of an epoxide (PSDVB@epoxy-Co). The synthesized adsorbents were thoroughly analyzed using ATR-IR, TGA, and SEM. By comparing EDS data, cobalt could be verified, and the amount quantified by ICP-MS. Next, the adsorptions of PFOA and PFOS at low concentrations of 20 µg L<sup>-1</sup> were investigated in an equilibrium state by using LC-MS. Here, both tested materials showed remarkable adsorption of up to 97 % for PFOA and PFOS. Furthermore, an increase in adsorption upon an ionic matrix of commercial drinking water and an adsorbent preference at different pH levels was demonstrated. By analyzing the influence of the concentration, resulting isotherms indicated multilayer adsorption, best described by a BET mechanism. Moreover, by measuring the total PFOA capacity by

adsorption in flow, a 4–5-fold increase was found compared to the novel material, leading to capacities of 215 mg g $^{-1}$  for PSDVB@APTES-Co and 296 mg g $^{-1}$  for PDSVB@epoxy-Co. By comparing the cobalt content to the adsorbed PFOA, we confirmed a BET mechanism for the adsorption of PFOA. Last, column-based adsorption experiments showed promising results at low (20  $\mu g~L^{-1}$ ) and medium concentrations (2.25 mg  $L^{-1}$ ). Reusability and regeneration studies found an excellent performance upon multiple cycles and best elution of up to 88  $\pm$  4 % by using ionic methanol.

### **Declaration of competing interest**

The authors declare that they have no known competing financial interests or personal relationships that could have appeared to influence the work reported in this paper.

### Acknowledgment

We thank Metrohm (Switzerland) for the donation of the particles. M.G. expresses his gratitude for the partial financial support provided by the European Union through the European Regional Development Fund (EFRE) and the State of Saarland, Germany, in the SWIMEMSYS project. M.G. is grateful for partial funding of this work in the framework of the cooperation platform iCARE for engineering sciences (Saarland). ICP-MS instrumentation for this work was provided by the Elemental Analysis Group, with financial support from Saarland University and the German Science Foundation (project number INST 256/553-1). The authors want to thank Aaron Haben for the ICP-MS measurements. The authors would like to thank Paul Fischer and Lukas Thörner for their excellent work on the LC-MS measurements.

### Appendix A. Supplementary data

Additional data on the column setup and preparation, elemental analysis results, data of BET determination, matrix composition of Evian water, further details in the calculation end evaluation of the BET adsorption mechanism, and additional SEM and EDS analysis before and after adsorption experiments. Supplementary data to this article can be found online at https://doi.org/10.1016/j.desal.2025.119018.

#### Data availability

Data will be made available on request.

#### References

- R. Dhore, G.S. Murthy, Per/polyfluoroalkyl substances production, applications and environmental impacts, Bioresour. Technol. 341 (2021) 125808, https://doi. org/10.1016/j.biortech.2021.125808.
- [2] S. Verma, T. Lee, E. Sahle-Demessie, M. Ateia, M.N. Nadagouda, Recent advances on PFAS degradation via thermal and nonthermal methods, Chem. Eng. J. Adv. 13 (2022) 1–11, https://doi.org/10.1016/j.ceja.2022.100421.
- [3] K.A. Barzen-Hanson, S.C. Roberts, S. Choyke, K. Oetjen, A. McAlees, N. Riddell, R. McCrindle, P.L. Ferguson, C.P. Higgins, J.A. Field, Discovery of 40 classes of perand polyfluoroalkyl substances in historical aqueous film-forming foams (AFFFs) and AFFF-impacted groundwater, Environ. Sci. Technol. 51 (4) (2017) 2047–2057, https://doi.org/10.1021/acs.est.6b05843.
- [4] Y. Zhi, H. Lu, K.D. Grieger, G. Munoz, W. Li, X. Wang, Q. He, S. Qian, Bioaccumulation and translocation of 6:2 fluorotelomer sulfonate, GenX, and perfluoroalkyl acids by urban spontaneous plants, ACS ES&T Engineering 2 (2022) 1169–1178, https://doi.org/10.1021/acsestengg.1c00423.
- [5] M.N. Ehsan, M. Riza, M.N. Pervez, M.M.O. Khyum, Y. Liang, V. Naddeo, Environmental and health impacts of PFAS: sources, distribution and sustainable management in North Carolina (USA), Sci. Total Environ. 878 (2023) 163123, https://doi.org/10.1016/j.scitotenv.2023.163123.
- [6] S. Roy, J. Moran, K. Danasekaran, K. O'Brien, S. Dakshanamurthy, Large-scale screening of per- and polyfluoroalkyl substance binding interactions and their mixtures with nuclear receptors, Int. J. Mol. Sci. 25 (15) (2024) 8241, https://doi. org/10.3390/ijms25158241.
- [7] S. Das, A. Ronen, A review on removal and destruction of per- and polyfluoroalkyl substances (PFAS) by novel membranes, Membranes 12 (7) (2022) 662, https:// doi.org/10.3390/membranes12070662.
- [8] R.A. Dickman, D.S. Aga, A review of recent studies on toxicity, sequestration, and degradation of per-and polyfluoroalkyl substances (PFAS), J. Hazard. Mater. 436 (2022) 129120, https://doi.org/10.1016/j.jhazmat.2022.129120.
- [9] D.P. Siriwardena, R. James, K. Dasu, J. Thorn, R.D. Iery, F. Pala, D. Schumitz, S. Eastwood, N. Burkitt, Regeneration of per- and polyfluoroalkyl substance-laden granular activated carbon using a solvent based technology, J. Environ. Manage. 289 (2021) 112439, https://doi.org/10.1016/j.jenvman.2021.112439.
- [10] B. Sonmez Baghirzade, Y. Zhang, J.F. Reuther, N.B. Saleh, A.K. Venkatesan, O. G. Apul, Thermal regeneration of spent granular activated carbon presents an opportunity to break the forever PFAS cycle, Environ. Sci. Technol. 55 (9) (2021) 5608–5619, https://doi.org/10.1021/acs.est.0c08224.
- [11] C.T. Vu, T. Wu, Recent progress in adsorptive removal of per- and poly-fluoroalkyl substances (PFAS) from water/wastewater, Crit. Rev. Environ. Sci. Technol. 52 (1) (2020) 90–129, https://doi.org/10.1080/10643389.2020.1816125.
- [12] H. Guo, Y. Liu, W. Ma, L. Yan, K. Li, S. Lin, Surface molecular imprinting on carbon microspheres for fast and selective adsorption of perfluorooctane sulfonate, J. Hazard. Mater. 348 (2018) 29–38, https://doi.org/10.1016/j. ihazmat.2018.01.018.
- [13] F. Cao, L. Wang, Y. Yao, F. Wu, H. Sun, S. Lu, Synthesis and application of a highly selective molecularly imprinted adsorbent based on multi-walled carbon nanotubes for selective removal of perfluorooctanoic acid, Environ. Sci.: Water Res. Technol. 4 (5) (2018) 689–700, https://doi.org/10.1039/c7ew00443e.
- [14] G.B. Post, P.D. Cohn, K.R. Cooper, Perfluorooctanoic acid (PFOA), an emerging drinking water contaminant: a critical review of recent literature, Environ. Res. 116 (2012) 93–117, https://doi.org/10.1016/j.envres.2012.03.007.
- [15] S. Tsuda, Les jeunes et les écrans: données récentes, J. Toxicol. Sci. 41 (2016) SP27–SP36, https://doi.org/10.2131/jts.41.SP27.

- [16] S. Saikat, I. Kreis, B. Davies, S. Bridgman, R. Kamanyire, The impact of PFOS on health in the general population: a review, Environ. Sci. Process. Impacts 15 (2) (2013) 329–335, https://doi.org/10.1039/c2em30698k.
- [17] K. Fu, J. Huang, F. Luo, Z. Fang, D. Yu, X. Zhang, D. Wang, M. Xing, J. Luo, Understanding the selective removal of perfluoroalkyl and polyfluoroalkyl substances via fluorine-fluorine interactions: a critical review, Environment Science & Technology 58 (2024) 16669–16689, https://doi.org/10.1021/acsest.4c06519.
- [18] A. Yousefi, K. Moradi, P. Karami, M.D. Firouzjaei, M. Elliott, A. Rahimpour, M. Sadrzadeh, Evaluating the efficiency of modified hydrophobic PVDF membrane for the removal of PFOA substances from water by direct contact membrane distillation, Desalination 579 (2024) 117509, https://doi.org/10.1016/j. desal.2024.117509.
- [19] W.A. Sheppard, The electronic properties of fluoroalkyl groups. Fluorine p-π interaction 1, J. Am. Chem. Soc. 87 (11) (2002) 2410–2420, https://doi.org/10.1021/ja01089a020.
- [20] W. Cai, D.A. Navarro, J. Du, P. Srivastava, Z. Cao, G. Ying, R.S. Kookana, Effect of heavy metal co-contaminants on the sorption of thirteen anionic per- and polyfluoroalkyl substances (PFAS) in soil, Sci. Total Environ. 905 (2023) 167188, https://doi.org/10.1016/j.scitotenv.2023.167188.
- [21] J.A. Sleep, S.J. Miklavcic, A.L. Juhasz, Modelling of PFAS-surface interactions: effect of surface charge and solution ions, Chemosphere 319 (2023) 137910, https://doi.org/10.1016/j.chemosphere.2023.137910.
- [22] Y. Gao, S.T. Le, T.C.G. Kibbey, W. Glamore, D.M. O'Carroll, A fundamental model for calculating interfacial adsorption of complex ionic and nonionic PFAS mixtures in the presence of mixed salts, Environ. Sci. Process. Impacts 25 (11) (2023) 1830–1838, https://doi.org/10.1039/d2em00466f.
- [23] F. Dixit, R. Dutta, B. Barbeau, P. Berube, M. Mohseni, PFAS removal by ion exchange resins: a review, Chemosphere 272 (2021) 129777, https://doi.org/ 10.1016/j.chemosphere.2021.129777.
- [24] S. Woodard, J. Berry, B. Newman, Ion exchange resin for PFAS removal and pilot test comparison to GAC, Remediat. J. 27 (3) (2017) 19–27, https://doi.org/ 10.1002/rem.21515.
- [25] E. Gagliano, M. Sgroi, P.P. Falciglia, F.G.A. Vagliasindi, P. Roccaro, Removal of poly- and perfluoroalkyl substances (PFAS) from water by adsorption: role of PFAS chain length, effect of organic matter and challenges in adsorbent regeneration, Water Res. 171 (2020) 115381, https://doi.org/10.1016/j.watres.2019.115381.
- [26] F.A. Zeidabadi, E.B. Esfahani, S.T. McBeath, M. Mohseni, Managing PFAS exhausted ion-exchange resins through effective regeneration/electrochemical process, Water Res. 255 (2024) 121529, https://doi.org/10.1016/j. watres.2024.121529.
- [27] H. Alyasi, S. Wahib, T.A. Gomez, K. Rasool, K.A. Mahmoud, The power of MXene-based materials for emerging contaminant removal from water a review, Desalination 586 (2024) 117913, https://doi.org/10.1016/j.desal.2024.117913.
- [28] L.I. FitzGerald, J.F. Olorunyomi, R. Singh, C.M. Doherty, Towards solving the PFAS problem: the potential role of metal-organic frameworks, Chemistry-Sustainability-Energy-Material 15 (19) (2022) e202201136, https://doi.org/10.1002/cssc 202201136
- [29] P. Baldaguez Medina, V. Ardila Contreras, F. Hartmann, D. Schmitt, A. Klimek, J. Elbert, M. Gallei, X. Su, Investigating the electrochemically driven capture and release of long-chain PFAS by redox metallopolymer sorbents, ACS Appl. Mater. Interfaces 15 (18) (2023) 22112–22122, https://doi.org/10.1021/ acsami.3c01670.
- [30] H.B. Gray, Y.S. Sohn, N. Hendrickson, Electronic structure of metallocenes, J. Am. Chem. Soc. 93 (15) (2002) 3603–3612, https://doi.org/10.1021/ja00744a011.
- [31] X. Su, K.-J. Tan, J. Elbert, C. Rüttiger, M. Gallei, T.F. Jamison, T.A. Hatton, Asymmetric faradaic systems for selective electrochemical separations, Energ. Environ. Sci. 10 (5) (2017) 1272–1283, https://doi.org/10.1039/c7ee00066a.
- [32] S. Schöttner, R. Hossain, C. Rüttiger, M. Gallei, Ferrocene-modified block copolymers for the preparation of smart porous membranes, Polymers (Basel). 9 (10) (2017) 491, https://doi.org/10.3390/polym9100491.
- [33] D. Schmitt, A. Schiesser, M. Gallei, Balance of hydrophilicity and hydrophobicity of stimuli-responsive metallopolymer-decorated organic particles, ACS Appl. Polym. Mater. 6 (5) (2024) 2993–3002, https://doi.org/10.1021/acsapm.4c00060.
- [34] D. Schmitt, M. Gallei, Redox-mediated ion separation and exchange by tailored design of immobilized metallopolymers, Desalination 583 (2024) 117674, https://doi.org/10.1016/j.desal.2024.117674.
- [35] C. Rüttiger, S. Mehlhase, S. Vowinkel, G. Cherkashinin, N. Liu, C. Dietz, R.W. Stark, M. Biesalski, M. Gallei, Redox-mediated flux control in functional paper, Polymer 98 (2016) 429–436, https://doi.org/10.1016/j.polymer.2016.01.065.
- [36] D.P. Puzzo, A.C. Arsenault, I. Manners, G.A. Ozin, Electroactive inverse opal: a single material for all colors, Angew. Chem. Int. Ed. 48 (5) (2009) 943–947, https://doi.org/10.1002/anie.200804391.
- [37] M. Gallei, C. Rüttiger, Recent trends in metallopolymer design: redox-controlled surfaces, porous membranes, and switchable optical materials using ferrocenecontaining polymers, Chemistry 24 (40) (2018) 10006–10021, https://doi.org/ 10.1002/chem.201800412.
- [38] J. Elbert, M. Gallei, C. Rüttiger, A. Brunsen, H. Didzoleit, B. Stühn, M. Rehahn, Ferrocene polymers for switchable surface wettability, Organometallics 32 (20) (2013) 5873–5878, https://doi.org/10.1021/om400468p.
- [39] N.L. Abbott, G.M. Whitesides, Potential-dependent wetting of aqueous solutions on self-assembled monolayers formed from 15-(ferrocenylcarbonyl)pentadecanethiol on gold, Langmuir 10 (5) (2002) 1493–1497, https://doi.org/10.1021/ la00017a029.
- [40] T. Rittner, K. Ghulam, M. Koch, M. Gallei, Amine-containing block copolymers for efficient catalyst-free hydroamination and preparation of functional

- metallopolymers, Polym. Chem. 15 (35) (2024) 3519–3528, https://doi.org/
- [41] T. Rittner, S. Pusse, B. Boßmann, K. Staudt, A. Haben, R. Kautenburger, H.P. Beck, M. Gallei, Metallopolymer-based block copolymers for perfluorinated substances (PFAS) and ion removal, J. Mater. Chem. C 12 (47) (2024) 19116–19129, https://doi.org/10.1039/d4tc03546a.
- [42] T. Rittner, J. Kim, A. Haben, R. Kautenburger, O. Janka, J. Kim, M. Gallei, One-pot functionalization for the preparation of cobaltocene-modified redox-responsive porous microparticles, Chem. Eur. J. 30 (2024) e202402338, https://doi.org/ 10.1002/chem.202402338.
- [43] F. Ahangaran, A.H. Navarchian, Recent advances in chemical surface modification of metal oxide nanoparticles with silane coupling agents: a review, Adv. Colloid Interface Sci. 286 (2020) 102298, https://doi.org/10.1016/j.cis.2020.102298.
- [44] S.P. Pujari, L. Scheres, A.T. Marcelis, H. Zuilhof, Covalent surface modification of oxide surfaces, Angewante Chemie International Edition 53 (25) (2014) 6322–6356, https://doi.org/10.1002/anie.201306709.
- [45] W. Zhang, E.P.C. Lai, Chemical functionalities of 3-aminopropyltriethoxy-silane for surface modification of metal oxide nanoparticles, Silicon 14 (2021) 6535–6545, https://doi.org/10.1007/s12633-021-01477-7.
- [46] H.M.M. Hesse, B. Zeeh, Infrared and Raman Characteristic Group Frequencies, 4 edn, John Wiley & Sons, 2004.
- [47] N. Majoul, S. Aouida, B. Bessaïs, Progress of porous silicon APTES-functionalization by FTIR investigations, Appl. Surf. Sci. 331 (2015) 388–391, https://doi.org/10.1016/j.apsusc.2015.01.107.
- [48] D. Schmitt, S.M. Abdel-Hafez, M. Tummeley, V. Schünemann, M. Schneider, V. Presser, M. Gallei, Surface-initiated living anionic polymerization of functional methacrylates from the surface of organic particles, Macromolecules 56 (17) (2023) 7086–7101, https://doi.org/10.1021/acs.macromol.3c01257.
- [49] C. Rüttiger, V. Pfeifer, V. Rittscher, D. Stock, D. Scheid, S. Vowinkel, F. Roth, H. Didzoleit, B. Stühn, J. Elbert, E. Ionescu, M. Gallei, One for all: cobalt-containing polymethacrylates for magnetic ceramics, block copolymerization, unexpected electrochemistry, and stimuli-responsiveness, Polym. Chem. 7 (5) (2016) 1129–1137, https://doi.org/10.1039/c5pv01845e.
- [50] V. Rittscher, M. Gallei, A convenient synthesis strategy for microphase-separating functional copolymers: the cyclohydrocarbosilane tool box, Polym. Chem. 6 (31) (2015) 5653–5662, https://doi.org/10.1039/c5py00065c.
- [51] J. Elbert, H. Didzoleit, C. Fasel, E. Ionescu, R. Riedel, B. Stühn, M. Gallei, Surface-initiated anionic polymerization of [1]silaferrocenophanes for the preparation of colloidal preceramic materials, Macromol. Rapid Commun. 36 (7) (2015) 597–603, https://doi.org/10.1002/marc.201400581.
- [52] E. Jonescu, H.J. Kleebe, R. Riedel, Silicon-containing polymer-derived ceramic nanocomposites (PDC-NCs): preparative approaches and properties, Chem. Soc. Rev. 41 (15) (2012) 5032–5052, https://doi.org/10.1039/c2cs15319j.
- [53] M. Briesenick, M. Gallei, G. Kickelbick, High-refractive-index polysiloxanes containing naphthyl and phenanthrenyl groups and their thermally cross-linked resins, Macromolecules 55 (11) (2022) 4675–4691, https://doi.org/10.1021/acs. macromol.2c00265.
- [54] D. Schmitt, O. Janka, R. Leiner, G. Kickelbick, M. Gallei, Preparation of preceramic ferrocene-modified microparticles for the development of uniform porous iron oxide particles and their sustainable recycling, Mater. Adv. 5 (7) (2024) 3037–3050, https://doi.org/10.1039/d3ma01131c.
- [55] G. Mera, M. Gallei, S. Bernard, E. Ionescu, Ceramic nanocomposites from tailor-made preceramic polymers, Nanomaterials (Basel) 5 (2015) 468–540, https://doi.org/10.3390/nano5020468.

- [56] R. Kautenburger, H.P. Beck, Influence of geochemical parameters on the sorption and desorption behaviour of europium and gadolinium onto kaolinite, J. Environ. Monit. 12 (6) (2010) 1295–1301, https://doi.org/10.1039/b914861b.
- [57] A.C. Umeh, M. Hassan, M. Egbuatu, Z. Zeng, M. Al Amin, C. Samarasinghe, R. Naidu, Multicomponent PFAS sorption and desorption in common commercial adsorbents: kinetics, isotherm, adsorbent dose, pH, and index ion and ionic strength effects, Sci. Total Environ. 904 (2023) 166568, https://doi.org/10.1016/j. scitoteny. 2023. 166568.
- [58] W. Cai, D.A. Navarro, J. Du, G. Ying, B. Yang, M.J. McLaughlin, R.S. Kookana, Increasing ionic strength and valency of cations enhance sorption through hydrophobic interactions of PFAS with soil surfaces, Sci. Total Environ. 817 (2022) 152975, https://doi.org/10.1016/j.scitotenv.2022.152975.
- [59] C. You, C. Jia, G. Pan, Effect of salinity and sediment characteristics on the sorption and desorption of perfluorooctane sulfonate at sediment-water interface, Environ. Pollut. 158 (5) (2010) 1343–1347, https://doi.org/10.1016/j.envpol.2010.01.009.
- [60] T. Zhu, S. Xu, A. Rahman, E. Dogdibegovic, P. Yang, P. Pageni, M.P. Kabir, X. D. Zhou, C. Tang, Cationic metallo-polyelectrolytes for robust alkaline anion-exchange membranes, Angewante Chemie International Edition 57 (9) (2018) 2388–2392, https://doi.org/10.1002/anie.201712387.
- [61] J. Zhang, J. Yan, P. Pageni, Y. Yan, A. Wirth, Y.P. Chen, Y. Qiao, Q. Wang, A. W. Decho, C. Tang, Anion-responsive metallopolymer hydrogels for healthcare applications, Sci. Rep. 5 (2015) 11914, https://doi.org/10.1038/srep11914.
- [62] T. Ito, T. Kenjo, Ion-exchange properties of anion-exchanger containing cobalticinium cations, Bull. Chem. Soc. Jpn. 41 (7) (1968) 1600–1605, https://doi. org/10.1246/bcsi.41.1600
- [63] E.A. Smith, W. Chen, How to prevent the loss of surface functionality derived from aminosilanes, Langmuir 24 (21) (2008) 12405–12409, https://doi.org/10.1021/ lag02234x
- [64] K.U. Goss, The p Ka values of PFOA and other highly fluorinated carboxylic acids, Environ. Sci. Technol. 42 (2) (2008) 456–458, https://doi.org/10.1021/ es702192c
- [65] I. Langmuir, Surface chemistry, Nobel Lecture (1932).
- [66] H. Freundlich, Über die adsorption in Lösungen, Z. Phys. Chem. 57U (1907) 385–470, https://doi.org/10.1515/zpch-1907-5723.
- [67] M.K. Beyer, Lehrbuch der Physikalischen Chemie. 6. Auflage, mit Arbeitsbuch von Gerd Wedler und Hans-Joachim Freund, Angew. Chem. 125 (2013) 3893, https://doi.org/10.1002/ange.201300430.
- [68] A. Ebadi, J.S. Soltan Mohammadzadeh, A. Khudiev, What is the correct form of BET isotherm for modeling liquid phase adsorption? Adsorption 15 (1) (2009) 65–73, https://doi.org/10.1007/s10450-009-9151-3.
- [69] S. Brunauer, P.H. Emmett, E. Teller, Adsorption of gases in multimolecular layers, J. Am. Chem. Soc. 60 (2) (2002) 309–319, https://doi.org/10.1021/ja01269a023.
- [70] Water Quality Determination Of Selected Per- And Polyfluoroalkyl Substances In Drinking Water - Method Using Liquid Chromatography/Tandem-mass Spectrometry (LC-MS/MS), DIN EN 17892, 2024-08, 10.31030/3547211.
- [71] J. Gandhi, N.H. Subramanian, Trace-level determination of perfluorinated compounds in water by suppressed ion chromatography with inline matrix elimination, Metrohm, 8.000.6053EN, https://www.metrohm.com/content/dam/ metrohm/shared/documents/technical-posters/80006053EN.pdf.
- [72] A. Zaggia, L. Conte, L. Falletti, M. Fant, A. Chiorboli, Use of strong anion exchange resins for the removal of perfluoroalkylated substances from contaminated drinking water in batch and continuous pilot plants, Water Res. 91 (2016) 137–146, https://doi.org/10.1016/j.watres.2015.12.039.